Mon. Not. R. Astron. Soc. **000**, 1–25 (2012) Printed 20 August 2012 (MN LATEX style file v2.2)

The ATLAS^{3D} project – XX. Mass-size and Mass-σ projections of the Virial Plane of early-type galaxies: variation of morphology, kinematics, mass-to-light ratio and stellar initial mass function

Michele Cappellari,[1⋆] Richard M. McDermid,[2] Katherine Alatalo,[3] Leo Blitz,[3] Maxime Bois,[4] Frédéric Bournaud,[5] M. Bureau,[1] Alison F. Crocker,[6] Roger L. Davies,[1] Timothy A. Davis,[1,7] P. T. de Zeeuw,[7,8] Pierre-Alain Duc,[5] Sadegh Khochfar,[10] Davor Krajnović,[7] Harald Kuntschner,[7] Raffaella Morganti,[11,12] Thorsten Naab,[13] Tom Oosterloo,[11,12] Marc Sarzi,[14] Nicholas Scott,[1,15] Paolo Serra,[11] Anne-Marie Weijmans[16] and Lisa M. Young[17]

[1] *Sub-department of Astrophysics, Department of Physics, University of Oxford, Denys Wilkinson Building, Keble Road, Oxford OX1 3RH*
[2] *Gemini Observatory, Northern Operations Centre, 670 N. A'ohoku Place, Hilo, HI 96720, USA*
[3] *Department of Astronomy, Campbell Hall, University of California, Berkeley, CA 94720, USA*
[4] *Observatoire de Paris, LERMA and CNRS, 61 Av. de l'Observatoire, F-75014 Paris, France*
[5] *Laboratoire AIM Paris-Saclay, CEA/IRFU/SAp CNRS Université Paris Diderot, 91191 Gif-sur-Yvette Cedex, France*
[6] *Department of Astrophysics, University of Massachusetts, 710 North Pleasant Street, Amherst, MA 01003, USA*
[7] *European Southern Observatory, Karl-Schwarzschild-Str. 2, 85748 Garching, Germany*
[8] *Sterrewacht Leiden, Leiden University, Postbus 9513, 2300 RA Leiden, the Netherlands*
[9] *Université Lyon 1, Observatoire de Lyon, Centre de Recherche Astrophysique de Lyon and Ecole Normale Supérieure de Lyon, 9 avenue Charles André, F-69230 Saint-Genis Laval, France*
[10] *Max-Planck Institut für extraterrestrische Physik, PO Box 1312, D-85478 Garching, Germany*
[11] *Netherlands Institute for Radio Astronomy (ASTRON), Postbus 2, 7990 AA Dwingeloo, The Netherlands*
[12] *Kapteyn Astronomical Institute, University of Groningen, Postbus 800, 9700 AV Groningen, The Netherlands*
[13] *Max-Planck Institut für Astrophysik, Karl-Schwarzschild-Str. 1, 85741 Garching, Germany*
[14] *Centre for Astrophysics Research, University of Hertfordshire, Hatfield, Herts AL1 9AB, UK*
[15] *Centre for Astrophysics & Supercomputing, Swinburne University of Technology, PO Box 218, Hawthorn, VIC 3122, Australia*
[16] *Dunlap Institute for Astronomy & Astrophysics, University of Toronto, 50 St. George Street, Toronto, ON M5S 3H4, Canada*
[17] *Physics Department, New Mexico Institute of Mining and Technology, Socorro, NM 87801, USA*

Submitted to MNRAS on 17 August 2012

ABSTRACT

In the companion Paper XIX of this series we derive accurate total mass-to-light ratios $(M/L)_{\rm JAM} \equiv [M/L](r = R_{\rm e})$ within a sphere of radius $r = R_{\rm e}$ centred on the galaxy, as well as stellar $(M/L)_{\rm stars}$ (with the dark matter removed) for the volume-limited and nearly mass selected (stellar mass $M_\star \gtrsim 6 \times 10^9 M_\odot$) ATLAS$^{\rm 3D}$ sample of 260 early-type galaxies (ETGs, ellipticals Es and lenticulars S0s). Here we use those parameters to study the two orthogonal projections $(M_{\rm JAM}, \sigma_e)$ and $(M_{\rm JAM}, R_e^{\rm max})$ of the thin Virial Plane (VP) $(M_{\rm JAM}, \sigma_e, R_e^{\rm max})$ which describes the distribution of the galaxy population, where $M_{\rm JAM} \equiv L \times (M/L)_{\rm JAM} \approx M_\star$. The distribution of galaxy properties on both projections of the VP is characterized by (i) a boundary in the galaxy distribution, described by two power-laws, joined by a break at a characteristic mass $M_{\rm JAM} \approx 3 \times 10^{10} M_\odot$, which corresponds to the minimum $R_{\rm e}$ and maximum stellar density, and (ii) a characteristic mass $M_{\rm JAM} \approx 2 \times 10^{11} M_\odot$ which separates a population dominated by fast rotator with disks at lower masses, from one dominated by quite round slow rotators at larger masses. The distribution of ETGs properties on the two projections of the VP tends to be constant along lines of constant σ_e, or constant $\sqrt{GM_\star/(5R_{\rm e}^{\rm max})} \approx \sigma_e$ respectively, and forms a continuous and parallel sequence with the distribution of spiral galaxies. This applies to the dynamical $(M/L)_{\rm JAM}$ and to other indicators of the $(M/L)_{\rm pop}$ of the stellar population, like $H\beta$ and colour, as well as to galaxy concentration, which we show is tracing the bulge mass. A similar variation along contours of σ_e is also observed for the mass normalization of the stellar Initial Mass Function (IMF), which was recently shown to vary systematically within the ETGs galaxy population. Our preferred relation has the form $\log_{10}[(M/L)_{\rm stars}/(M/L)_{\rm Salp}] = a + b \times \log_{10}(\sigma_e/130{\rm km\,s^{-1}})$ with $a = -0.11 \pm 0.01$ and $b = 0.36 \pm 0.06$. This trend implies a transition of the mean IMF from Kroupa to Salpeter in the interval $\log_{10}(\sigma_e/{\rm km\,s^{-1}}) \approx 1.9 - 2.4$ (or $\sigma_e \approx 80 - 260$ km s^{-1}), with a smooth variation in between, consistently with what was shown in Cappellari et al. (2012). The observed distribution of galaxy properties on the VP provides a clean and novel view for a number of previously reported trends, which constitute special two-dimensional projections of the more general four-dimensional parameters trends on the VP. We interpret the distribution of galaxy properties on the VP as due to a combination of two main effects: (i) an increase of the bulge fraction, with a corresponding increase of the concentration and decrease in $R_{\rm e}$, which seems connected to the quenching of star formation, and (ii) dry merging, increasing galaxy mass and $R_{\rm e}$ by moving galaxies along lines of roughly constant σ_e (or steeper), while leaving the population unchanged.

Key words: galaxies: elliptical and lenticular, cD – galaxies: evolution – galaxies: formation – galaxies: structure – galaxies: kinematics and dynamics

1 INTRODUCTION

Much of our understanding of galaxy formation and evolution comes from the study of dynamical scaling relations relating galaxy luminosity or mass, size and kinematic (e.g. Faber & Jackson 1976; Kormendy 1977; Dressler et al. 1987; Faber et al. 1987; Djorgovski & Davis 1987) or regular trends in the distribution of galaxy properties as a function of their scaling parameters (e.g. Bender et al. 1992; Burstein et al. 1997; Kauffmann et al. 2003b; Gallazzi et al. 2006), and from the study of their evolution with redshift (e.g. van Dokkum & Franx 1996; Kelson et al. 1997; van Dokkum et al. 1998; Treu et al. 2005; Franx et al. 2008).

The volume-limited ATLAS$^{\rm 3D}$ sample of nearby early-type galaxies (Cappellari et al. 2011a, hereafter Paper I) constitute an ideal benchmark for studying scaling relations and the distribution of galaxy properties, given the availability of a high-quality multi-wavelength dataset. In particular in **?**, hereafter Paper XIX we used the state-of-the-art integral-field kinematics to derive accurate masses and global dynamical parameter. We found that galaxies lie, with very good accuracy, on a thin Virial Plane (VP) describing galaxies in the parameter space defined by mass, velocity dispersion and projected half-light radius $(M_{\rm JAM}, \sigma_e, R_e^{\rm max})$. The existence of this plane is due to the virial equilibrium condition

$$M_{\rm JAM} \propto \sigma_e^2 R_e^{\rm max} \quad (1)$$

and for this reason by itself it contains no useful information on galaxy formation. All the useful constraints on galaxy formation models come from the inhomogeneous distribution of galaxies in non-edge-on views of the VP and from the distribution of galaxy properties along the VP.

This paper is devoted to a study of the non edge-on projections of the VP to see what we learn from it on galaxy formation. This is done in the spirit of the classic papers by Bender et al. (1992) and Burstein et al. (1997). However the fact that we have accurate dynamical masses implies that our VP is extremely thin and it follows the virial equations quite accurately. For this reason we can ignore edge-on views of the plane and focus on non edge-on projections only. The thinness of the VP implies that any inclined projection show essentially the same information, after a change of coordinates. We can use standard and easy-to-understand observables as our main coordinates, instead of trying to observe the plane at a precisely face-on view.

* E-mail: cappellari@astro.ox.ac.uk

In this paper, in Section 2 we summarize the sample and data, in Section 3 we present our projections of the VP. We illustrate the distribution of a number of quantities on the (M, σ_e) and (M, R_e) projection. We show the variation of the $(M/L)_{\rm JAM}$, as well as of population indicators of M/L. We show the variation of galaxy concentration, intrinsic shape, morphology and stellar rotation. The variations of the IMF are separately presented in Section 4, together with a review of previous results on the IMF variation. in Section 5 we discuss the implications of our findings for galaxy formation and briefly summarize our paper in Section 6.

2 SAMPLE AND DATA

2.1 Selection

The galaxies studied in this work are the 260 early-type galaxies which constitute the volume-limited and nearly mass-selected ATLAS^{3D} sample (Paper I). The object were morphologically selected as early-type according to the standard criterion (Hubble 1936; de Vaucouleurs 1959; Sandage 1961) of not showing spiral arms or a disk-scale dust lane (when seen edge-on). The early-types are extracted from a parent sample of 871 galaxies of all morphological types brighter than $M_K = -21.5$ mag, using 2MASS photometry (Skrutskie et al. 2006), inside a local ($D < 42$ Mpc) volume of 1.16×10^5 Mpc^3 (see full details in Paper I).

In Paper XIX we compared our sample to previous samples for which accurate dynamical masses have been determined either via gravitational lensing (e.g. Bolton et al. 2008b; Auger et al. 2010a) or dynamics (e.g. Magorrian et al. 1998; Cappellari et al. 2006; Thomas et al. 2009) and conclude that it provides a major step forward in sample size and accuracy.

2.2 Stellar kinematics and imaging

Various multi-wavelengths datasets are available for the sample galaxies (see a summary in Paper I). In this work we make use of the SAURON (Bacon et al. 2001) integral-field stellar kinematics within about one half-light radius R_e, which was introduced in Emsellem et al. (2004), for the subset of 48 early-types in the SAURON survey (de Zeeuw et al. 2002). The kinematics of all galaxies in the ATLAS^{3D} sample was homogeneously extracted as described in Paper I, using the pPXF software (Cappellari & Emsellem 2004) and the full MILES stellar library (Sánchez-Blázquez et al. 2006; Falcón-Barroso et al. 2011) as templates.

Effective velocity dispersions σ_e were measured by co-adding all the spectra in the SAURON datacube contained within the half-light isophote, or within the largest observed aperture. The resulting "effective spectrum" was still fitted with pPXF using the full MILES stellar library as templates, and assuming a Gaussian line-of-sight velocity distribution. Gas emission around the possible Hβ and $[OIII]$ emission lines were systematically excluded from the fits and the CLEAN keyword of pPXF was used to reject possible remaining outliers from the spectra.

The photometry used in this work comes from the Sloan Digital Sky Survey (SDSS, York et al. 2000) data release eight (DR8 Aihara et al. 2011) and was supplemented by our own photometry taken at the 2.5-m Isaac Newton Telescope in the same set of filters and with comparable signal to noise for the rest of the sample galaxies (Scott et al. 2012, hereafter Paper XXI).

2.3 Measuring galaxy global parameters: M/L, R_e and σ_e

The dynamical masses used in this paper were obtained with the dynamical models of the ATLAS^{3D} sample presented in Cappellari et al. (2012) and described in more detail in Paper XIX. In brief the modelling approach starts by approximating the observed SDSS and INT r-band surface brightness distribution of the ATLAS^{3D} galaxies using the Multi-Gaussian Expansion (MGE) parametrization (Emsellem et al. 1994), with the fitting method and software of Cappellari (2002)[1]. Full details of the approach and examples of the resulting MGE fits are given in Paper XXI. The MGE models are used as input for the Jeans Anisotropic MGE (JAM) modelling method[1] which calculates a prediction of the line-of-sight second velocity moments $\langle v_{\rm los}^2 \rangle$ for a given set of model parameters and fits this to the observed $V_{\rm rms}$ (Cappellari 2008) using a Bayesian approach (Gelman et al. 2004). The models include a spherical dark halo, which is parametrised according to six different sets of assumptions (See Paper XIX for full details). In Cappellari et al. (2012) we showed that the adopted assumptions on the halo have insignificant influence on the measured trend of M/L. For this reason in this paper we only use the two simplest sets of models from that paper (using the same notation):

(A) Self-consistent axisymmetric JAM model, in which the dark matter is assumed to be proportional to the stellar one. We call the total (luminous plus dark) M/L of this model $(M/L)_{\rm JAM}$;
(B) Axisymmetric JAM model with spherical Navarro et al. (1996) (NFW) dark matter halo. Here the M/L of the stars alone $(M/L)_{\rm stars}$ is measured directly.

Lablanche et al. (2012, hereafter Paper XII) studied the accuracy in the M/L obtained with the JAM method, using N-body simulations that resemble real galaxies, and concluded that the M/L of unbarred galaxies can be measured with negligible bias $< 1.5\%$, while the M/L of barred galaxies that resemble typical bars found in the ATLAS^{3D} sample can bias the determination by up to 15% in our tests, depending on the position angle of the bars.

The M/L of the stellar population $(M/L)_{\rm Salp}$ in the SDSS r-band was presented in Cappellari et al. (2012). It was extracted using the penalized pixel-fitting (pPXF) method and software of Cappellari & Emsellem (2004) for full spectrum fitting. In this case the model templates consisted of a regular rectangular grid of 26 ages and 6 metallicities $[M/H]$, assuming a Salpeter (1955) IMF for reference, from the MILES models of Vazdekis et al. (2010). We used the pPXF keyword REGUL to enforce linear regularization (Press et al. 1992, eq. 18.5.10) in the recovered set of templates weights from the fit. The regularization parameter was chosen for every galaxy to obtain an increase $\Delta\chi^2 = \sqrt{2 \times N_{\rm pix}}$ in the χ^2, with respect to a non-regularized fit. In this way the recovered solution constitutes the smoothest one consistent with the observed spectrum (see fig. 20 of Onodera et al. 2012 for an example). This regularized approach helps reducing the noise in the $(M/L)_{\rm Salp}$ determination, however the results are quite insensitive to the precise value of this parameter and remain essentially unchanged for a range of plausible values. More details on our spectral fitting of the SAURON data and the resulting star formation histories will be presented in McDermid et al. (in preparation).

Effective radii are defined as the projected half-light radii of the isophote containing half of the total analytic light of the MGE models from Paper XXI. Both circularized radii R_e and the more robust major axes $R_e^{\rm max}$ were extracted as described in Paper XIX.

[1] Available from http://purl.org/cappellari/idl

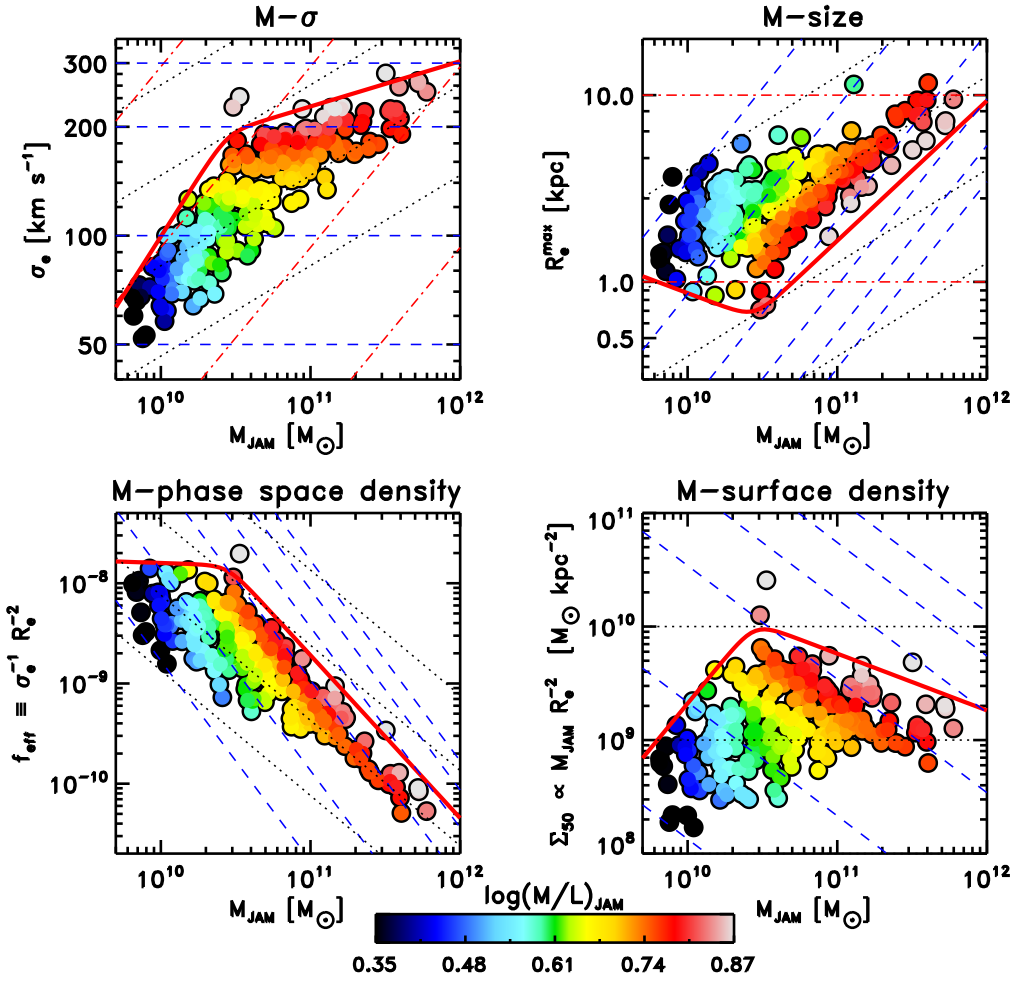

Figure 1. The Virial Plane and it projections. The top two panels show the two main projections of the VP in the $(M_{\rm JAM}, \sigma_e)$ and $(M_{\rm JAM}, R_e^{\rm max})$ coordinates. Overlaid are lines of constant $\sigma_e = 50, 100, 200, 300, 400, 500$ km s^{-1} (dashed blue), constant $R_e^{\rm max} = 0.1, 1, 10, 100$ kpc (dot-dashed red) and constant $\Sigma_e = 10^8, 10^9, 10^{10}, 10^{11}\ M_\odot$ kpc^{-2} (dotted black) *predicted* by the virial relation. The observed $(M_{\rm JAM}, \sigma_e, R_e^{\rm max})$ points follow the relation so closely that the coordinates provide a unique mapping on these diagram and one can reliably infer all characteristics of the galaxies from any individual projection. In each panel the galaxies are coloured according to the (LOESS smoothed) $\log(M/L)_{\rm JAM}$, as shown in the colour bar at the bottom. Moreover in all panels the thick red line shows the ZOE relation given by equation (3), again projected according to the virial relation $M_{\rm JAM} = 5.0 \times \sigma_e^2 R_e^{\rm max}/G$. While the top two panels contain different observable quantities, the bottom two panels merely apply a coordinate transformation to the quantities in the top two panels, to show the effective phase space density $f_{\rm eff} \equiv 1/(\sigma {R_{\rm e}}^2)$ and effective mass surface density $\Sigma_e \equiv M_{\rm JAM}/(2\pi {R_{\rm e}}^2)$. Two galaxies stand out for being significantly above the ZOE in the $(M_{\rm JAM}, \sigma_e)$ and $(M_{\rm JAM}, \Sigma_e)$ projections. The top one is NGC 5845 and the bottom one is NGC 4342.

3 PROJECTIONS OF THE VIRIAL PLANE

3.1 Total M/L variations

We have shown in Paper XIX that the existence of the FP is almost entirely due, with good accuracy, to a virial equilibrium condition combined with a smooth variation in M/L. Once this is clarified, the edge-on projection of the Virial Plane becomes uninteresting from the point of view of the study of galaxy formation, as it merely states an equilibrium condition satisfied by galaxies and it does not encode any memory of the formation process itself. This is in agreement with previous findings with simulations (Nipoti et al. 2003; Boylan-Kolchin et al. 2006). All information provided by scaling relations on galaxy formation is now encoded in the non edge-on projections of the Virial Plane, and first of all in the distribution of M/L on that plane. In Paper XIX we also confirmed that M/L correlates remarkably tightly with σ_e (Cappellari et al. 2006). This is especially true (i) for slow rotators, (ii) for galaxies in clusters and (iii) at the high-end of the σ_e range. Here we look at the entire Virial Plane and try to clarify the reason for these and other galaxy correlations.

In a classic paper Bender et al. (1992) studied the distribution of hot stellar systems in a three-dimensional space, they called κ space, defined in such a way that one of the axes was empirically defined to lie nearly orthogonal to the plane. This made it easy to look at both the edge-on and face-on versions of the plane. In this paper, thanks to the availability of state-of-the-art integral-field kinematics and the construction of detailed dynamical models, we can use mass as one of the three variables $(M_{\rm JAM}, \sigma_e, R_{\rm e})$. We have shown that in these variables the plane is extremely thin and follows the scalar virial equation $M_{\rm JAM} = 5.0 \times \sigma_e^2 R_e^{\rm max}/G$ within our tight errors. This implies that any projection of the plane contains the same amount of information, except for a change of coordinates. Instead of looking at the plane precisely face-on, we decided to construct special projections that correspond to physically-meaningful and easy-to-interpret quantities.

Our selection of meaningful projections of the VP is shown in Fig. 1. We use as horizontal axis in all plots our main mass variable

$$M_{\rm JAM} \equiv L \times (M/L)_{\rm JAM} \approx 2 \times M_{1/2} \approx M_{\rm stars}, \quad (2)$$

where $(M/L)_{\rm JAM}$ is the total (luminous plus dark) dynamical M/L obtained using self-consistent JAM models, L is the total galaxy luminosity and $M_{1/2}$ is the total mass within a sphere of radius $r_{1/2}$ enclosing half of the total galaxy light, where $r_{1/2} \approx 1.33R_{\rm e}$ (Hernquist 1990; Ciotti 1991; Wolf et al. 2010, Paper XIX). Although the self-consistency assumption, where the total mass is proportional to the stellar mass, is not justified at large radii, it is accurate within the region where we have stellar kinematics (about $1R_{\rm e}$). It was shown in Williams et al. (2010) and in Paper XIX that $(M/L)_{\rm JAM}$ closely reproduces the total $(M/L)(r = R_{\rm e})$ inside a sphere (actually an iso-surface) with mean radius the projected half-light radius $R_{\rm e}$, derived using models which explicitly include dark matter. Different assumptions on the dark halo produce minor differences in $(M/L)(r = R_{\rm e})$. Given that $(M/L)(r = R_{\rm e})$ is nearly insensitive to the choice of the halo assumptions, we choose the self-consistent one, being the simplest.

As illustrated in Paper XIX (see also Williams et al. 2009), most of the galaxies in our sample are consistent with having small fractions of dark matter within a sphere of radius $r = R_{\rm e}$, with a median value of just 12% of DM within that radius for our standard models (B). This implies that $M_{1/2}$ is dominated by the stellar mass. For this reason $M_{\rm JAM}$ is a quantity that very closely represents and is directly comparable to the total stellar galaxy mass used in numerous previous studies. Stellar mass seems to relate well with galaxy properties and is often used to study galaxy formation (e.g. Kauffmann et al. 2003a,b; Hyde & Bernardi 2009b). The difference of our mass parameter is that it does not suffer from the uncertainties related to the stellar population models (e.g. Maraston et al. 2006; Gallazzi & Bell 2009; Conroy et al. 2009; Longhetti & Saracco 2009; Wuyts et al. 2009) moreover it automatically includes the effects of a non-universal IMF (van Dokkum & Conroy 2010; Cappellari et al. 2012). Being a measure of the total enclosed mass within a spherical region, and thus being directly related the dynamics, $M_{\rm JAM}$ represents the ideal parameter which one would like to use in scaling relations. Note that $M_{\rm JAM}$, unlike mass determinations obtained via strong lensing, does not include the possible contribution of dark matter along the cylinder parallel to the line-of-sight (Dutton et al. 2011a), which provides an useful additional constraint on dark matter at large radii, but complicates the interpretation of scaling relations in the galaxy centres.

In the top-left and top-right panels of Fig. 1 we show the projections of the VP along the $(M_{\rm JAM}, \sigma_e)$ axes. The colour in these diagrams represent the dynamical M/L inside a sphere of radius $R_{\rm e}$. Three important results are clear from these plots:

(i) Both projections are equivalent and provide basically the same picture, apart from a coordinate transformation. This is expected from the tightness of the VP. Moreover, given that the VP nearly follows the virial relation, one can plot virial coordinates defined by $M_{\rm JAM} = 5.0 \times \sigma_e^2 R_{\rm e}/G$, to construct a consistent and accurate system of coordinates in both panels to infer other dynamical quantities;

(ii) Galaxies define a clear zone-of-exclusion (ZOE), as already discovered by Bender et al. (1992) and Burstein et al. (1997), however we find a clear break at a mass $M \approx 3 \times 10^{10} M_\odot$ and two nearly power-law regimes above or below this value. The ZOE is approximated by the equation

$$R_{\rm e} = R_{\rm e,b} \left(\frac{M_{\rm JAM}}{M_{\rm JAM,b}}\right)^{\gamma} \left[\frac{1}{2} + \frac{1}{2}\left(\frac{M_{\rm JAM}}{M_{\rm JAM,b}}\right)^{\alpha}\right]^{(\beta-\gamma)/\alpha} \quad (3)$$

with $R_{\rm e,b} = 0.7$ kpc, $\alpha = 8$, $\beta = 0.75$, $\gamma = -0.30$. The relation has an asymptotic trend $R_{\rm e} \propto M_{\rm JAM}^{0.75}$ above $M_{\rm JAM,b} = 2.8 \times 10^{10} M_\odot$, and a sharp transition into $R_{\rm e} \propto M_{\rm JAM}^{-0.30}$ below this break. The values were determined by simultaneously matching the observed boundary in the galaxy distribution in all VP projections. These values are close to those already reported in Paper I (eq. 4 there), using K-band luminosity in place of mass and 2MASS $R_{\rm e}$ instead of MGE ones. The maximum in the galaxy density at $M_{\rm JAM,b}$ that we infer from our sample is also clearly visible in the much larger SDSS sample of (van Dokkum et al. 2008, fig. 2). This shows that the relation is robust. The ZOE relation can be converted into a $(M_{\rm JAM}, \sigma_e)$ one, or into other projections using the scalar virial relation $M_{\rm JAM} = 5.0 \times \sigma_e^2 R_e^{\rm max}/G$. The location of the break we find agrees with the value at which scaling relations of large sample of SDSS galaxies show a subtle deviation from a straight line (Hyde & Bernardi 2009a). Interestingly in both cases the characteristic mass at the cusp coincides with the value reported by Kauffmann et al. (2003b), as the fundamental dividing line between the two distinct families of passive and star-forming galaxies.

(iii) The contours of constant $(M/L)_{\rm JAM}$ closely follow lines of constant σ_e above $\sigma_e \gtrsim 100$ km s^{-1}. A comparable agreement is reached using lines parallel to the ZOE $R_e^{\rm max} \propto M_{\rm JAM}^{0.75}$. Neither mass $M_{\rm JAM}$, nor size $R_{\rm e}$ or surface mass density Σ_e provide a comparably good approximation to the $(M/L)_{\rm JAM}$ contours, although Σ_e provides a better approximation than the other two. This is consistent and explains the finding by Cappellari et al. (2006) that σ_e and not mass or luminosity, is the best tracer of $(M/L)_{\rm JAM}$. At lower $\sigma_e \lesssim 100$ km s^{-1} the $(M/L)_{\rm JAM}$ contours start deviating from the lines of constant σ and tend to lie closer to lines of constant $M_{\rm JAM}$. Given that the M/L describes the deviations between the FP and the VP, this twist in the contours demonstrates that the FP is warped with respect to the VP, and explains the sensitivity of the FP parameters to the region included in the fit (D'Onofrio et al. 2008; Gargiulo et al. 2009; Hyde & Bernardi 2009b).

Two galaxies stand out for being significantly above the ZOE in the $(M_{\rm JAM}, \sigma_e)$ and $(M_{\rm JAM}, \Sigma_e)$ projections. The top one is NGC 5845 and the bottom one is NGC 4342. The two objects have very high surface brightness and consequently excellent kinematic and photometric data. They are genuine examples of dense objects in the nearby Universe. These two outliers were already presented in Cappellari (2011a) and their compactness was later discussed by Jiang et al. (2012). However they have smaller masses ($M_{\rm JAM} \approx 3 \times 10^{10}\ M_\odot$) than their high-redshift counterparts (Cimatti et al. 2008; van Dokkum et al. 2008). In all panels of Fig. 1 the measured $(M/L)_{\rm JAM}$ have been adaptively smoothed using the Locally Weighted Regression robust technique (dubbed LOESS) of Cleveland (1979), straightforwardly generalized to two dimension as in Cleveland & Devlin (1988). In all plots we adopt a regularization factor $f = 0.3$, and a linear local approximation, which implies that a fraction 30% of the points are adopted every time for the tricube-weighted robust fit of a local plane. To deal with the different scales of the axes, and the elongated relations, before applying LOESS we re-normalize the coordinates so that their ellipsoid of inertia reduces to a circle. We do not show here the original data, as the scatter in $(M/L)_{\rm JAM}$ is already analysed in detail in Paper XIX. Given that most of the variation in the smooth surface happens orthogonally to the constant σ_e lines, the scatter from the smooth surface of 27% is nearly unchanged from the value of 29%

in the global $(M/L) - \sigma_e$ relation, further confirming that all the variation happens orthogonally to σ_e.

In the bottom left and right panels of Fig. 1 we show the effective phase-space density, defined following Hernquist et al. (1993) as $f_{\rm eff} \equiv 1/(\sigma_e {R_{\rm e}}^2)$ and the mass surface density, defined as $\Sigma_e \equiv M_{\rm JAM}/(2\pi {R_{\rm e}}^2)$. Note that, while we use $R_e^{\rm max}$ for the mass-size plane, one has to use $R_{\rm e}$ for Σ_e. The two bottom panels do not plot new data, but are obtained by rearranging the three variables shown in the top panels, however they illustrate how the above trends relate to other physical quantities. In particular the phase-space density is interesting because it can only decrease during collisionless galaxy mergers, due to Liouville's theorem (Carlberg 1986; Hernquist et al. 1993). Interestingly the ZOE we find is nearly flat in $f_{\rm eff}$ below $M_{\rm JAM,b} = 3 \times 10^{10} M_\odot$ (a value $\gamma = 1/3$ gives $f_{\rm eff} = {\rm const}$ in the virial case) and starts decreasing at larger masses, as one would expect when dry mergers start becoming more important.

3.2 Stellar population indicators of $(M/L)_{\rm pop}$

We have shown in Paper XIX that the stellar matter dominates in the regions we study. If this is indeed the case we would expect stellar population indicators of the $(M/L)_{\rm pop}$ of the stellar population to closely follow the behaviour of the dynamical $(M/L)_{\rm JAM}$. Before addressing this question with our own data, the reader is strongly encouraged to compare Fig. 1 to the right panel of figure 15 of Gallazzi et al. (2006), which shows the luminosity-weighted age versus the stellar mass in the $(\sigma, M_\star)$ projection. Even though Fig. 1 uses dynamical quantities, which are measured via dynamical models, while Gallazzi et al. (2006) derives population from line strengths, the two plots resemble each other very closely, including the change of orientation of the contours around $\sigma \sim 100$ km s^{-1}. This comparison already indicates a close link between M/L and stellar population (mainly age), in broad agreement with Cappellari et al. (2006). Importantly, given that our sample is 100 times smaller than the one of Gallazzi et al. (2006), this comparison also confirms the ability of the LOESS technique to recover the underlying distribution from our smaller galaxy sample.

We now address the relation between dynamical and population M/L using our own dataset and a different approach. Two main simple tracers of $(M/L)_{\rm pop}$ have been proposed in the past: (i) the $B-R$ colour, which was shown by (Bell & de Jong 2001) to trace $(M/L)_{\rm pop}$ alone, for a wide range of metallicities, and (ii) the line-strength index $H\beta$, which was shown to satisfy a similar property in Cappellari et al. (2006) for a wide range of metallicities (see also Worthey 1994). Here we adopt the $H\beta$ determination for our ATLAS$^{\rm 3D}$ galaxies, as derived from the very high S/N effective SAURON spectra. The parameters for the SAURON survey (de Zeeuw et al. 2002) subset of 48 galaxies was already given in Kuntschner et al. (2006). The homogeneous extraction for the ATLAS$^{\rm 3D}$ sample will be given in McDermid et al. (in preparation). As choice of colour we use the SDSS $g-i$ one, which is available for 223 ATLAS$^{\rm 3D}$ galaxies in SDSS DR8 and was shown by Gallazzi & Bell (2009) to provide on average the smallest uncertainties and the most stable results, among the SDSS bands.

The results are presented in Fig. 2 and show a quite good agreement between simple population estimators of M/L and the dynamical one. Both $H\beta$ and colour are nearly constant along lines of constant σ as it was the case for Fig. 1. This confirms the fact that the key driver of the total M/L is the stellar population. We do notice some systematic differences at the low-σ end, with the contours of constant $(M/L)_{\rm pop}$ not quite following the population trends. As the effect is visible both in colour and $H\beta$ we believe it is significant. It may be due to the presence of extended star formation episodes, which are expected to be more prevalent at low mass (Heavens et al. 2004; Thomas et al. 2005) and cause a break in the relation between population observables and M/L. The study of the relation between our parameters and the actual physical parameters of the population, like age, metallicity and abundance ratios, is presented in McDermid et al. (in preparation). Analysis of the stellar population parameters for the SAURON survey (de Zeeuw et al. 2002) subset of 48 galaxies was already presented in (Kuntschner et al. 2010).

3.3 Variations of galaxy concentration and morphology

In the previous sections we showed that galaxy properties follow smooth trends in the projections of the VP. We have seen that the dynamical M/L near the galaxy centre ($1R_{\rm e}$) is driven by a variation of the stellar population, with the dynamical M/L constituting an accurate tracer of the galaxy population! These trends distribute galaxies in the VP along lines of nearly constant σ_e. In Paper I we showed that the luminosity-size relation changes gradually with sizes decreasing as a function of the bulge ratio, indicated by the morphological classification. We interpreted the apparent size decrease as an actual increase of the bulge mass between different morphological types. In Paper II and III, we showed that the vast majority of local ETGs is constituted by disk-like systems, the fast rotators, and in (Cappellari et al. 2011b, hereafter Paper VII) we discussed how fast-rotators morphologically resemble spirals with a variety of bulge fractions. We concluded that fast rotators simply constitute the end point of a smooth sequence of disks with increasing bulges, and this lead us to propose a fundamental change in our view of galaxy morphology (Paper VII). If this picture is correct, we should be able to find an indication for a systematic change in the bulge fraction, in the fast rotators class, while moving from the region of the VP populated by spiral galaxies towards the ZOE, dominated by the oldest and reddest galaxies, with the largest M/L.

A detailed photometric bulge-disk decomposition of the unbarred galaxies subset of the ATLAS$^{\rm 3D}$ sample is presented Krajnović et al. (2012, hereafter Paper XVII). Although it provides a well established definition of the bulge luminosity, it is a complex technique which depends on the extraction details and may suffer from degeneracies. Moreover it is unclear how it should be applied to barred galaxies. For this reason here we look instead at the simple concentration parameter TGC (Trujillo et al. 2001). It measures the ratio between the flux within $1R_{\rm e}$ and $R_{\rm e}/3$ which we extracted from the MGE photometric models as described in Paper XIX. For a given galaxy mass an increase of the bulge fraction produces by definition a larger concentration. The distribution of galaxy concentrations on the VP is shown in the top panel of Fig. 3. Even though the values are noisier than the clean M/L trends, a systematic variation is evident, with galaxy concentration roughly following the M/L, $H\beta$ and $g-i$ colour trends, which all tend to be constant along lines of constant σ_e. This trend is consistent with the trends of concentration against Σ_e and σ_e reported by Graham et al. (2001b), and the corresponding correlation with supermassive black holes (Graham et al. 2001a). It is also consistent with a similar trend between M/L and Sersic (1968) index reported by D'Onofrio et al. (2011). Here we interpret all these trends as due to the increase of the bulge fraction, rather than a smooth change in the profile shape of a spheroidal system. It's important to stress that our term "bulge" refers to an increase of the mass fraction in the centre of the galaxy. It does not necessarily imply a correspondence with the definition

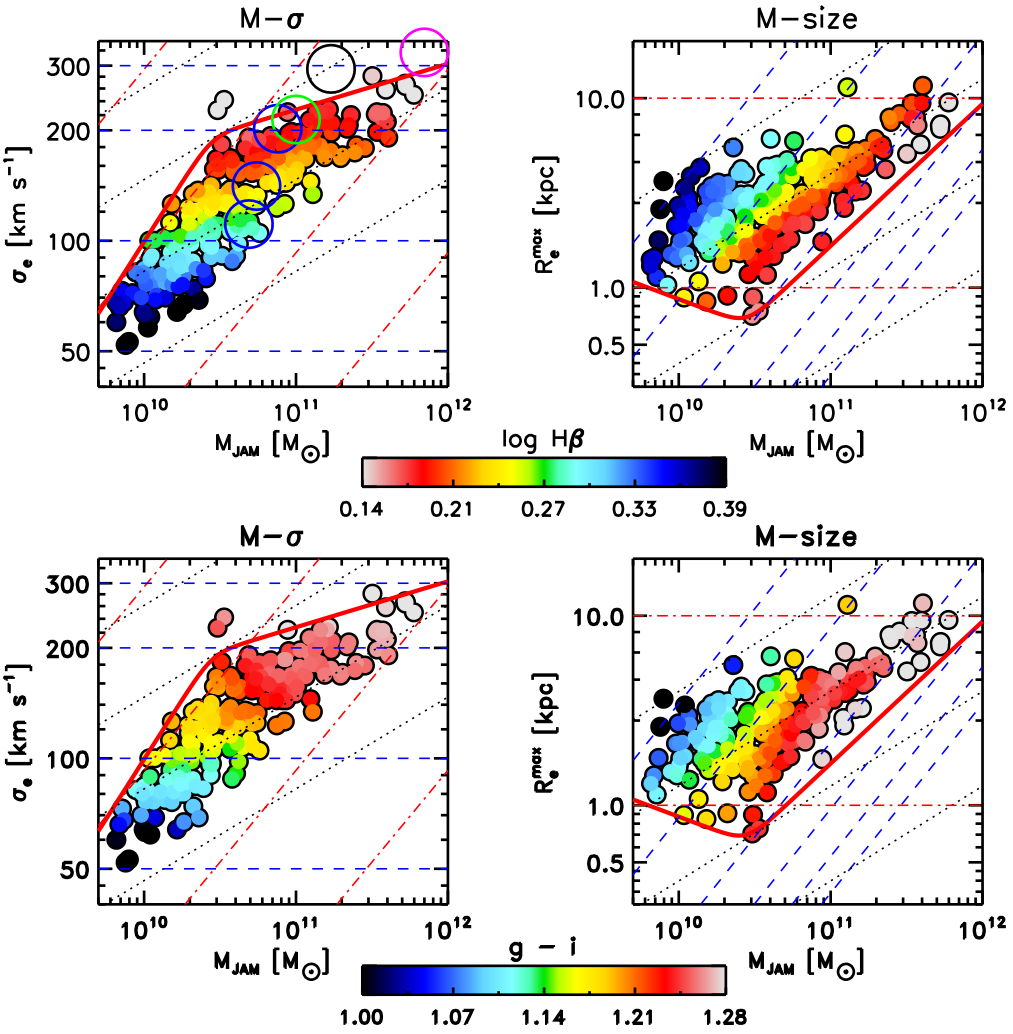

Figure 2. Indicators of $(M/L)_{\rm pop}$ on the Virial Plane. *Top Panels:* Same as in Fig. 1, with colours showing the $\log H\beta$ line-strength, from McDermid et al. (in preparation), which is a good indicator of $(M/L)_{\rm pop}$. The open circles represent σ determination for galaxies at redshift $z > 1.4$: blue symbols from Cappellari et al. (2009), green symbol from Cenarro & Trujillo (2009), magenta symbol from Onodera et al. (2012) and black symbol from (van de Sande et al. 2011). Not shown is the σ value from van Dokkum et al. (2009), which is off the vertical scale. *Bottom Panels:* Same as in Fig. 1, with colours indicating the SDSS galaxy colour $g-i$. Note that both $(M/L)_{\rm pop}$ and $g-i$ show the same trends as $(M/L)_{\rm JAM}$ in Fig. 1.

of "bulge" that one infers via classic bulge-disk decomposition (Paper XVII), namely a light excess over an outer exponential component. There is some evidence that the concentration may follow population even more closely than M/L, possibly due to the contribution of extended star formation episodes as we commented for Fig. 2.

The concentration plot demonstrates that indeed, even within the ETG class (excluding the few slow rotators), the variation of galaxy properties follows the bulge growth. Interestingly the plot also shows a slight decrease in the concentration at the largest mass end $M_{\rm JAM} \gtrsim 2 \times 10^{11} M_{\odot}$. This value coincides with another characteristic scale in ETGs, above which galaxies start to be rounder (Tremblay & Merritt 1996; van der Wel et al. 2009b), to have flat central profiles in their surface brightness (Faber et al. 1997; Graham 2004; Ferrarese et al. 2006) and to deviate from power-law colour-magnitude relations (Ferrarese et al. 2006; Bernardi et al. 2011).

3.4 Variations of galaxy intrinsic flattening and rotation

Our dynamical modelling effort provides the unique opportunity of having the galaxy inclination for the entire ATLAS^{3D} sample of galaxies. We verified that the JAM inclination agrees with the one inferred from the geometry of the dust, for 26 galaxies with regular dusts disks (see also Cappellari 2008). We further verified that we can recover with JAM models the inclination of simulated galaxies that resemble typical objects in our sample (Paper XII). Although one should not expect the inclination to be reliable for every individual galaxy, it is expected to be accurate for most of our sample. The inclination allows us to recover the intrinsic shape of individual objects. The deprojection is done using the ellipticity of the outer isophote, measured in Paper II at radii typically around $4R_{\rm e}$, at the depth limit of the SDSS photometry. We then computed the intrinsic ellipticity assuming an oblate spheroid geometry as (Binney & Tremaine 2008)

$$\varepsilon_{\rm intr} = 1 - \sqrt{1 + \varepsilon(\varepsilon - 2)/\sin^2 i}, \quad (4)$$

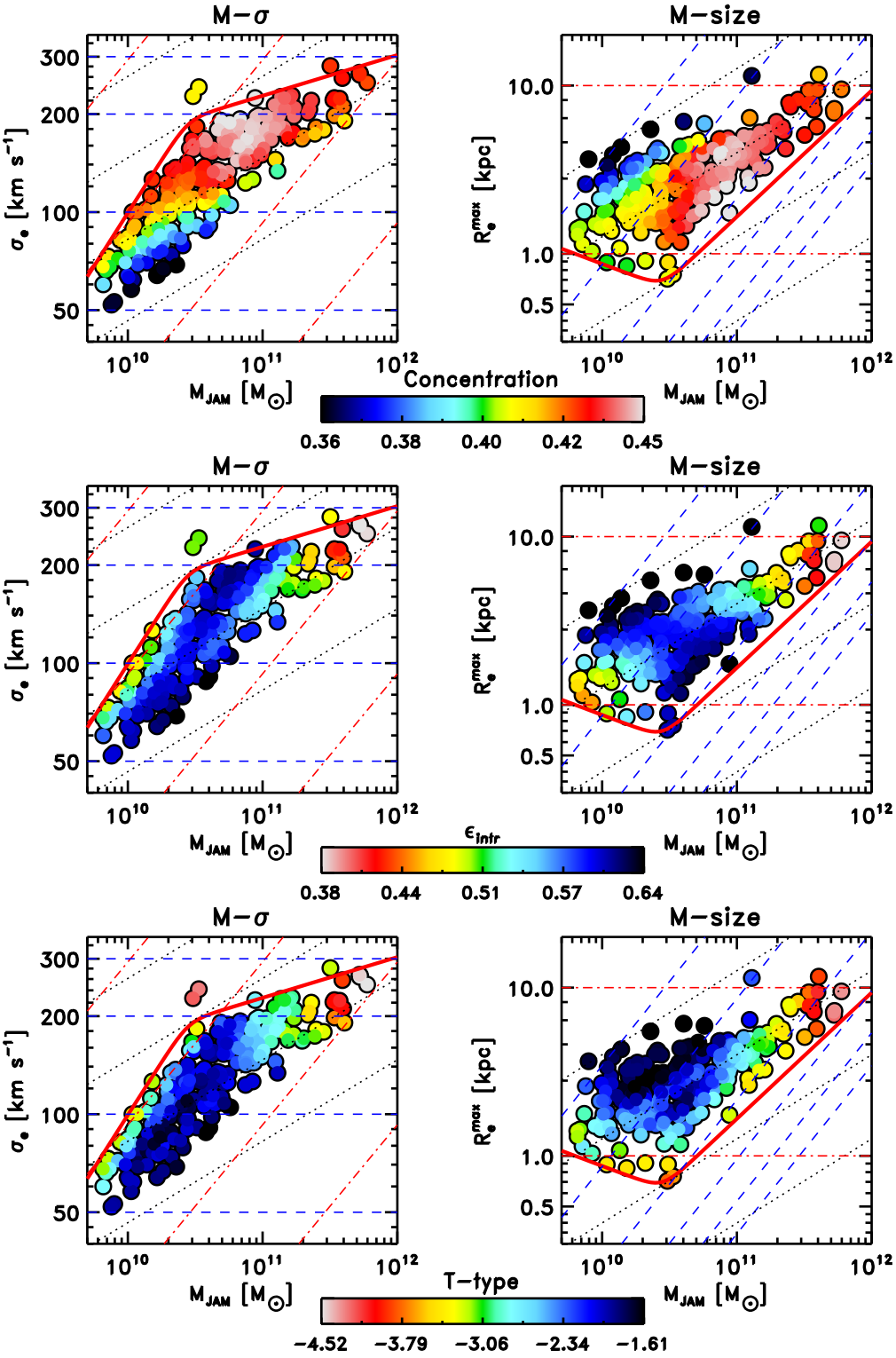

Figure 3. Concentration and shape on the Virial Plane. *Top Panels:* Same as in Fig. 1, with colours indicating the concentration parameter TGC of Trujillo et al. (2001). The trends are noisier than M/L but there is a clear increase in the concentration along lines of roughly constant σ_e and a slight decrease above a characteristic mass $M_{\rm JAM} \gtrsim 2\times10^{11}\,M_\odot$. *Middle Panels:* Same as in Fig. 1, with colours indicating the intrinsic ellipticity $\varepsilon_{\rm intr}$ of the galaxies outer regions, computed by de-projecting the observed ellipticity ϵ at large radii (Paper II) using the inclination inferred from the JAM models. Except again for the special region above $M_{\rm JAM} \gtrsim 2\times10^{11}\,M_\odot$, all the rest of the ETGs have on average the flattening of disks $\varepsilon \approx 0.65$ consistently with the Monte Carlo approach of Paper III, which suggests fast rotators have a typical intrinsic ellipticity $\varepsilon_{\rm intr} \approx 0.7$ and the statistical inversion in Weijmans et al. (in preparation).

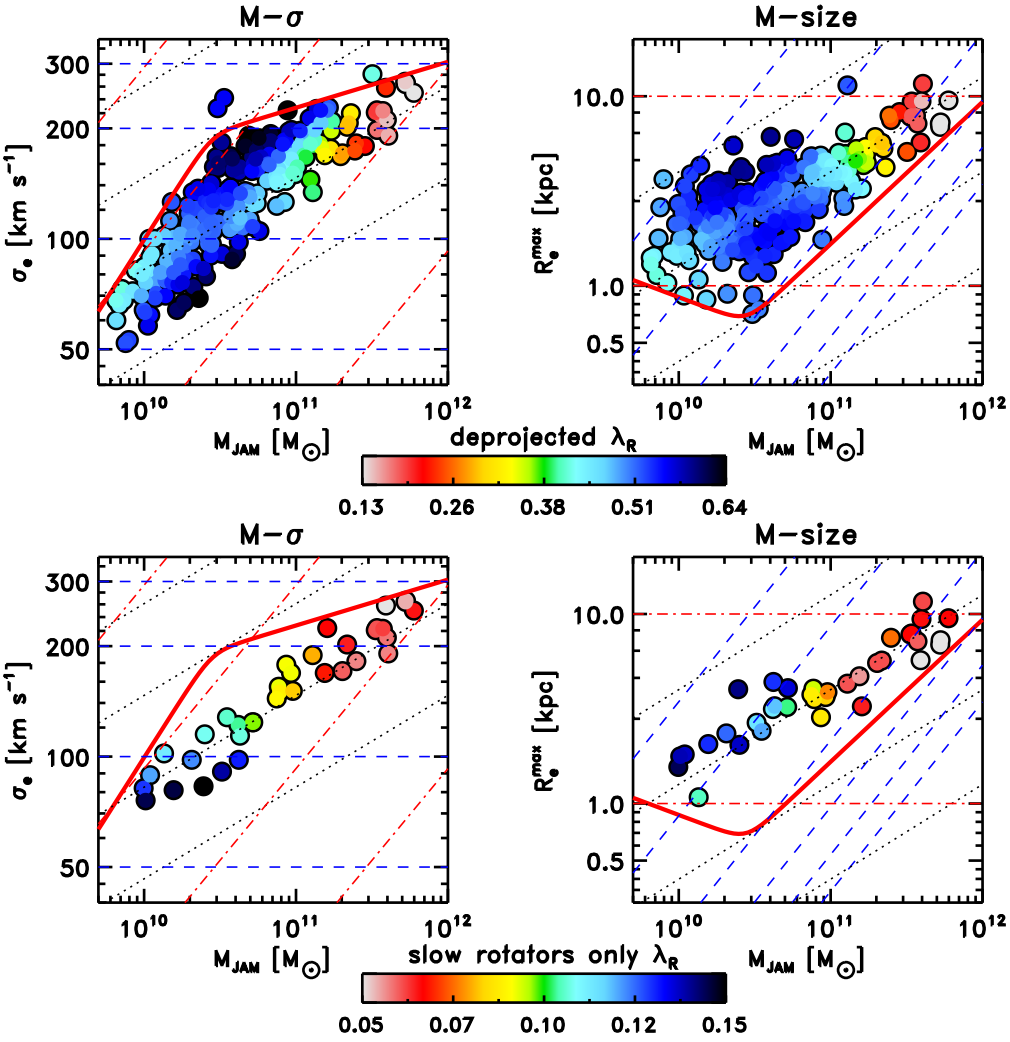

Figure 4. Same as in Fig. 1, with colours indicating the specific angular momentum parameter λ_R of (Emsellem et al. 2007), as given in Paper III. *Top Panels:* all ATLAS^{3D}galaxies are included. *Bottom Panels:* Only the slow rotators are shown. They seems to define a sequence in the VP, and they show a decrease in the rotation above $M_{\rm JAM} \gtrsim 2 \times 10^{11} M_{\odot}$.

The results of the deprojection is shown in the middle panels of Fig. 3. Contrary to all previous diagrams the distribution of the intrinsic ellipticity for ETGs on the VP shows a completely different trend. Few galaxies stand out in the top-right corner for being nearly round, with intrinsic ellipticity $\varepsilon_{\rm intr} \approx 0.2$. These galaxies are all located above the same characteristic mass $M_{\rm JAM} \gtrsim 2 \times 10^{11} M_{\odot}$, where the top panels showed a drop in the central density. This result confirms previous statistical studies of ETGs shapes (Tremblay & Merritt 1996; van der Wel et al. 2009b; Bernardi et al. 2011). Below this characteristic mass, the mean ellipticity drops dramatically and sharply to about $\varepsilon_{\rm intr} \approx 0.65$, characteristics of disks. This galaxy-by-galaxy shape deprojection confirms a similar result on their shape distribution inferred via Monte Carlo simulations from the distribution of fast rotators ETGs on the (λ_R, ε) diagram, suggesting fast rotators have a typical intrinsic ellipticity $\varepsilon_{\rm intr} \approx 0.7$ (fig. 15 in Paper III). It also agrees with a statistical inversion of their shape (Weijmans et al. in preparation). This agreement also seems to confirm the reliability of the inclinations derived via the JAM models. The result strongly confirms our previous conclusions that fast rotators as a class are disk like (Paper II, III, VII). The fact that the outer parts of fast rotators are as flat as disks, while the central ones show an increase of concentration, conclusively demonstrates that the latter is due to an increase of the *bulge* (or spheroid) mass, and not to the smooth variation of the profile in a spheroidal object which follows a $R^{1/m}$ profile. At the lowest mass range, near the ZOE, there seems to be a marginal decrease of $\varepsilon_{\rm intr}$. The significance or reality of this feature is however unclear.

The round and massive objects that stand out from the distribution are the prototypical slow rotators, which also stand out for their slow specific stellar angular momentum, as shown in Paper III. Another view of that fact is shown in the bottom panel of Fig. 3, which plots the angular momentum parameter λ_R of Emsellem et al. (2007) for the slow rotator ETGs only, as tabulated for the galaxies of the ATLAS^{3D} sample in Paper III. The slow rotators are found to populate a rather narrow sequence on the VP, with a small range of Σ_e. There is a clear trend of decreasing rotation with increasing mass as noted in Paper III, or possibly a sharp transition around $M_{\rm JAM} \approx 10^{11} M_{\odot}$, which is similar to the characteristic mass defined by concentration and intrinsic ellipticity. Although we tend to cover a smaller field with our kinematics for the largest galaxies, the qualitative difference in the kinematics for the most massive slow rotators is already clearly visible from the ve-

locity fields (Paper II) and it is not due to the difference in the field coverage.

In summary the distribution of galaxy properties on the $(M_{\rm JAM}, \sigma_e)$ and $(M_{\rm JAM}, R_e^{\rm max})$ projections of the Virial Plane can be understood as due to a smooth variation in the bulge mass as already suggested in figure 4 of Paper I. The connection between bulge mass and galaxy properties, and the close link between ETGs and spiral galaxies is further illustrated in Fig. 5, which includes the location of the spiral galaxies of the ATLAS$^{\rm 3D}$ parent sample (Paper I) together with the ETGs. The masses of spiral galaxies was approximately estimated assuming a fixed $M/L_K = 0.8\, M_\odot/L_\odot$, which ensures agreement between $M_{\rm JAM}$ and the K-band luminosity at the lowest masses. The plot shows that ETGs properties vary smoothly with those of spiral galaxies. Galaxies with negligible bulges are almost invariably star forming and classified as late spirals. Galaxies with intermediate bulges can still form stars and be classified as early-spirals, or can be fast rotator ETGs. But the galaxies with the most massive bulges, as indicated by their largest concentration or σ_e are invariably ETGs. They have the largest M/L (Fig. 1, the reddest colours and smallest Hβ (Fig. 2, but are still flat in their outer parts, indicating they have disks (Fig. 3) and generally still rotate fast (Fig. 4). An exception are galaxies with masses $M_{\rm JAM} \gtrsim 2 \times 10^{11}\, M_\odot$, which stand out for being nearly round, and non rotating.

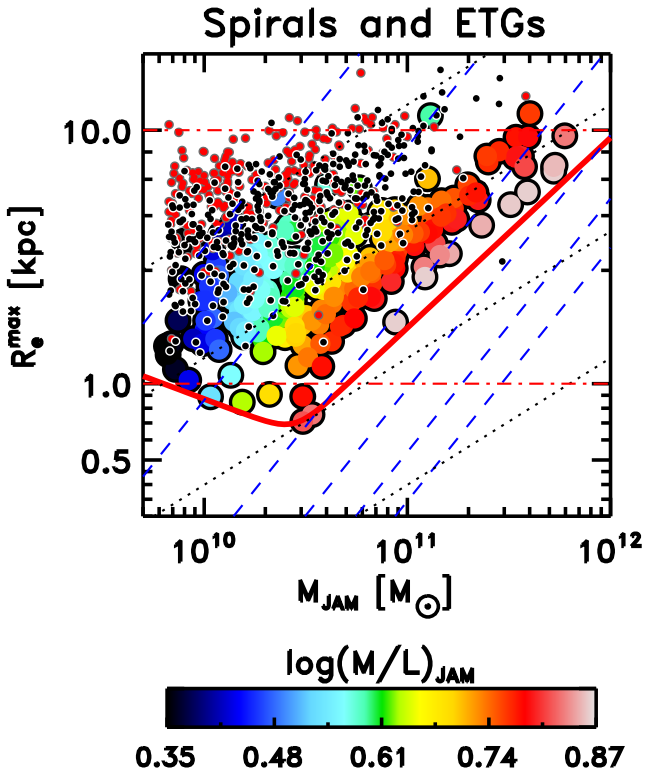

Figure 5. The Mass-size distribution for spiral galaxies and ETGs. The ETGs of the ATLAS$^{\rm 3D}$ sample are coloured according to their $(M/L)_{\rm JAM}$ as in Fig. 1. This plot however also includes the approximate location of spiral galaxies in the ATLAS$^{\rm 3D}$ parent sample, where masses are obtained from K-band luminosities, scaled to match $M_{\rm JAM}$ (a plot with both ETGs and spirals luminosities was shown in Paper I). Early spirals (Sa-Sb: $T \leq 4$) are indicated by the small black filled circles, while late spirals (Sc-Irr: $T > 4$) are shown with the small filled red circles. Late spirals are larger than ETGs, while early spirals overlap with the ETGs with low M/L. There are essentially no spirals in the region of the oldest and reddest ETGs, which have the largest M/L. This illustrates the fact that the increase of the spheroid is required to make a galaxy old and red and consequently produce the largest M/L.

4 SYSTEMATIC VARIATION OF THE IMF

Although the IMF variation could have been included among the other galaxy observables described in Section 3, we keep the IMF in a separate section for a more detailed coverage than for the other observables. In recent months there has been a large amount of interest on the IMF variation. Before describing our new ATLAS$^{\rm 3D}$ results, in the following section we provide a summary of this rapidly evolving field. To clarify the significance and robustness of the various recent claims, including our own, we place particular emphasis on the modelling assumptions that went into the various studies.

4.1 Summary of previous IMF results

4.1.1 IMF of the Milky Way

The stellar initial mass function (IMF) describes the distribution of stellar masses when the population formed. Nearly every aspect of galaxy formation studies requires a choice of the IMF to calculate predictions for galaxy observables (Kennicutt 1998). For this reason the IMF has been subjected to numerous investigations since the first determination more than half a century ago finding it has the form (Salpeter 1955)

$$\zeta(m) \propto m^x = m^{-2.3}, \qquad (5)$$

for $m > 0.4 M_\odot$, where m is the stellar mass.

In the Milky Way the IMF can be measured via direct stellar counts. Various determination in different environments lead to the finding of a remarkable universality in the shape of the IMF (Kroupa 2002), with the IMF being well described by the Salpeter power slope $x = -2.3$ for $m < 0.5 M_\odot$ and a shallower one at smaller masses $x = -1.3$ for $m \geq 0.5 M_\odot$ (Kroupa 2001). The Milky Way IMF can also be described by a log-normal distribution (Chabrier 2003), which has some theoretical justification. However the Kroupa and Chabrier IMFs are essentially indistinguishable from an observational point of view (Kroupa et al. 2012).

Recent IMF results were reviewed by Bastian et al. (2010) who concluded no clear evidence existed for a non-universal IMF in our galaxy and among different galaxies.

4.1.2 IMF from ionized gas emission or redshift evolution

In external galaxies individual stars cannot yet be resolved down to sufficiently small masses for IMF studies. Some indirect constraints on the slope of the IMF above $\sim 1 M_\odot$ can be obtained by combining observations of the Hα equivalent widths, which is related to the number of ionizing photons, with the galaxy colour, which is a function of the galaxy stellar population (Kennicutt 1998). Using this technique Hoversten & Glazebrook (2008) inferred a variation of the IMF with more massive galaxies having a more top-heavy IMF than Salpeter, a result confirmed under the same assumptions (Gunawardhana et al. 2011) by the GAMA survey (Driver et al. 2011).

Constraints on the IMF can also be obtained by comparing the local ($z = 0$) stellar mass density to the integral of the cosmic star formation history. Wilkins et al. (2008) finds that the local stellar mass density is lower than the value obtained from integrating

the cosmic star formation history (SFH), assuming that all the stars formed with a Salpeter IMF. They propose a time-variable IMF to reconcile the observations (see also Davé 2008).

Alternative constraints on the IMF can be obtained by studying the evolution of the M/L normalization in samples of galaxies as a function of redshift, for example from the evolution of the tilt and normalization of the Fundamental Plane with redshift (Renzini & Ciotti 1993). From these constraints and from the metal abundance in the clusters interstellar medium Renzini (2005) concluded that elliptical galaxies as a class must have an IMF close to Salpeter for stellar masses $m > 1M_{\odot}$, while the IMF must flatten at lower masses, similar to the Kroupa IMF.

A related approach was employed by van Dokkum (2008) who used the ratio of luminosity evolution to colour evolution of massive galaxies in clusters to constrain the IMF. He originally concluded that the IMF must be top heavy at high redshift, but this result was recently revised to conclude that the IMF above $m > 1M_{\odot}$ is actually not inconsistent with a Salpeter slope (van Dokkum & Conroy 2012).

4.1.3 Lensing or dynamics IMF constraints for external spirals

A more direct approach to constraining the variation of the IMF in galaxies consists of measuring the mass of the stars, and comparing this with the predictions of stellar population models. It is important to stress however that this method does not measure the shape of the IMF directly, but only its overall mass normalization. The method can only verify whether the stellar mass in a certain region within a galaxy is consistent with that due to a stellar population with a certain assumed IMF. Moreover these methods do not measure the same IMF one can infer via direct stellar counts in star clusters. They measure instead the stellar mass distribution due to the superposition of the IMFs from a large number of star clusters in the galaxy as well as the IMFs coming from the accretion of satellite galaxies during the galaxy hierarchical growth. As pointed out by Kroupa & Weidner (2003), even if the IMF was universal in every cluster in a galaxy, the integrated galactic IMF (IGIMF) would be different from the universal one, due to the non-uniform mass distribution of star clusters (see Kroupa et al. 2012, for an in-depth discussion). Hierarchical evolution complicates the picture even further. For these reason, when we state e. g. that "a galaxy is consistent with the Salpeter IMF", we simply imply, consistently with all previous similar studies, that "the galaxy has the same stellar M/L of a stellar population with the given age and metallicity (and abundances), and the Salpeter IMF".

The first convincing constraint on the IMF of external galaxies was obtained for a sample of 21 spiral galaxies, using the kinematics of the gas. Bell & de Jong (2001) concluded that *if the IMF is universal*, a sensible assumption at the time, it cannot have the Salpeter form, but it must be lighter, consistently with Kroupa-type. The result was later confirmed, still using gas kinematics, for a sample of 34 bright spiral galaxies by Kassin et al. (2006).

Th need for a light IMF was inferred for the Einstein Cross spiral galaxy gravitational lens system (Huchra et al. 1985) by both van de Ven et al. (2010) and Ferreras et al. (2010), and for another spiral lens galaxy by Suyu et al. (2012). As part of the DiskMass Survey (Bershady et al. 2010), which obtained integral-field stellar kinematics of a sample of 30 spiral galaxies, a light IMF was indirectly confirmed from the sub-maximality of the disks (Bershady et al. 2011). As part of the SWELLS survey of spiral lens galaxies (Treu et al. 2011) the need for a light IMF for most spiral galaxies was also found from the analysis of 20 strong gravitational lens (Brewer et al. 2012).

An inconsistency of the Salpeter IMF normalization for low mass galaxies was also inferred by Dutton et al. (2011b), using simple galaxy models with a bulge and a disk, trying to reproduce global trends for a large sample of galaxies extracted from the SDSS.

In summary there is a good agreement on the fact that spiral galaxies as a class must have a normalization lighter than Salpeter and similar to Kroupa/Chabrier. This is a robust result due to the fact that a Salpeter IMF would over-predict the total mass in the galaxy centres. It is unclear whether some spiral galaxies have a Salpeter IMFs, and of course whether the IMF varies within the galaxies themselves, as claimed by Dutton et al. (2012c).

4.1.4 Lensing or dynamics IMF constraints on early-types

An early attempt at constraining the IMF of 21 elliptical galaxies, using detailed spherical dynamical models including dark matter, found a general consistency between the stellar $(M/L)_{\rm stars}$ and the one of the population $(M/L)_{\rm pop}$, using the Kroupa IMF, but could not accurately constrain the IMF normalization due to large observational errors (Gerhard et al. 2001). A large study of SDSS elliptical galaxies using fixed spherical Hernquist galaxy models with dark halos (Padmanabhan et al. 2004) found a mass excess over the predictions of stellar population models with a fixed IMF, increasing with luminosity. This was interpreted as a increase of the dark matter fraction. A similar conclusion was reached by Zaritsky et al. (2006) while studying the fundamental manifold. A caveat of those studies was the use of homologous stellar profiles or approximate assumptions to study systematic variations in the heterogeneous galaxy population.

To overcome these limitations, as part of the SAURON project (de Zeeuw et al. 2002), we constructed self-consistent axisymmetric models reproducing in detail both the photometry and the state-of-the-art integral-field stellar kinematics data (Emsellem et al. 2004) for 25 early-type galaxies (Cappellari et al. 2006). The assumption that mass follows light is not accurate at large radii, but it is a good assumption for the region where kinematics is available ($\lesssim 1R_{\rm e}$), and provides accurate measurements of the total (luminous plus dark) M/L within a sphere of radius $r \approx R_{\rm e}$ (see Paper XIX). The resulting improvement in the M/L accuracy and the removal of systematic biases allowed us to strongly confirm that "the total and stellar M/L clearly do not follow a one-to-one relation. Dark matter is needed to explain the differences in M/L (if the IMF is not varying)" (Cappellari et al. 2006, see fig. 17 there). Although dark matter seemed, at the time, still a more natural explanation of our observations, if the measured trends are re-interpreted as an IMF variation, they would imply an IMF heavier than Salpeter for some of the oldest objects. That study also concluded that *if the IMF is universal* it must have a mass normalization as low as Kroupa IMF, consistently with the results for spiral galaxies, otherwise the stellar mass would overpredict the total one for a number of galaxies. A similar finding was obtained by Ferreras et al. (2008) using gravitational lensing of 9 elliptical galaxies extracted from the SLACS survey (Bolton et al. 2006).

A number of subsequent studies used approximate models reproducing the velocity dispersion of large galaxy samples to study dark matter and IMF variations in galaxies. Tortora et al. (2009) used spherical isotropic models with Sersic (1968) profiles to reproduce the large velocity dispersion compilation by Prugniel & Simien (1996). Graves & Faber (2010) used the Funda-

mental Plane of early-type galaxies from SDSS data. Schulz et al. (2010) combined weak lensing measurements in the outer parts to SDSS velocity dispersion determination, using spherical Jeans models with a Hernquist profile. All three studies confirmed the existence of a mass excess which increases with mass. They all preferred a dark matter trend to explain the observations, although they could not exclude the IMF variation alternative.

Grillo et al. (2009) compared stellar population masses, derived from multicolour photometry, to the total masses, inside the Einstein radius of the lenses, published by the SLACS team (Bolton et al. 2008a). He assumed for all galaxies the average dark matter fraction determined for some of the galaxies by Koopmans et al. (2006) and Gavazzi et al. (2007), which were based on spherical models assuming a single power-law total mass and a Hernquist (1990) (or Jaffe 1983) stellar profile. From this comparison Grillo et al. (2009) concluded that elliptical galaxies prefer a Salpeter rather than Kroupa/Chabrier IMF. The same result was found when comparing stellar dynamical masses for galaxies in the Coma cluster by Thomas et al. (2009), which includes the dark matter halo using fixed NFW profiles, to stellar population masses (Grillo & Gobat 2010). However, given that the dynamical masses were determined assuming a fixed NFW profile, the conclusion depended on the correctness of that assumption. A recent reanalysis of the 16 Coma galaxies by Thomas et al. (2011), still assuming a NFW dark halo profile, interpreted the M/L excess in massive galaxies as more likely due to dark matter, although their results are not inconsistent with a Salpeter IMF instead. A similar result was found by Wegner et al. (2012) for 8 galaxies in Abell 262.

The SLACS team analysed their data assuming all galaxies in their sample can be approximated by homologous spherical and isotropic systems with a Hernquist (1990) (or Jaffe 1983) profile. In Treu et al. (2010) they further assumed a spherical NFW profile for the dark matter, with fixed slope and only mass as free parameter. Given that the enclosed total (luminous plus dark) mass inside the Einstein radius is essentially fixed by the lens geometry, under these assumptions the central velocity dispersion is a unique function of the profile of the total mass distribution, which in this case is defined by a single parameter: the ratio between the stellar and dark matter components. Comparing the stellar mass from the lens model to the one from population, based on multicolour photometry (Auger et al. 2009), they found that the data prefer a Salpeter-like normalization of the IMF. Auger et al. (2010b) used the SLACS data and the same spherical Hernquist models but instead assumed that the halo mass for individual galaxies is known, as given by the abundance matching techniques, assuming a universal IMF (Moster et al. 2010). They still assumed NFW halos but explored both adiabatically contracted (Gnedin et al. 2004) and not contracted halos. They concluded that the data favour a Salpeter-like normalization of the IMF over a lighter Kroupa/Chabrier form.

Although ground-breaking, the analyses of the SLACS data depended on some non-obvious assumptions. Grillo et al. (2009) had assumed of a fixed dark matter fraction, as well as a power-law form for the total mass. Treu et al. (2010) result depended on the assumption of a fixed NFW halo slope, as the authors acknowledged concluding that "the degeneracy between the two [IMF or dark matter] interpretations cannot be broken without additional information, the data imply that massive early-type galaxies cannot have both a universal IMF and universal dark matter halos", in agreement with previous dynamical analyses. Auger et al. (2010b) result depended on assuming the halo mass from the abundance matching techniques. This led the authors to conclude that "better constraints on the star formation efficiency must be obtained from the data in order to draw definitive conclusions about the role of a mass-dependent IMF relative to CDM halo contraction".

Other independent studies of the same SLACS data did not exclude an IMF variation, but did not confirm the need for a Salpeter IMF to explain the observations. Tortora et al. (2010) reached this conclusion using spherical Hernquist isotropic models like Treu et al. (2010) and Auger et al. (2010b), but could not explain the reason for the disagreement. A similar study was also performed by Deason et al. (2012). They showed that the trend in the galaxies enclosed masses can be explained by a toy model similar to the one adopted by Auger et al. (2010b), but with a universal Kroupa IMF. Deason et al. (2012) study however did not fit the galaxies stellar velocity dispersion, which could be a reason for the difference in the results. Barnabè et al. (2011) re-analysed 16 SLACS galaxies using axisymmetric, rather than spherical, dynamical models, and describing the galaxy images in detail, rather than assuming fixed Hernquist profiles. Their models are fitted to integral-field stellar kinematics, instead of a single velocity dispersion. They find that the data are consistent with both a Kroupa or a Salpeter IMF, in agreement with the early study by Ferreras et al. (2008).

An additional limitation all previous analyses of the full SLACS sample was the assumption that all galaxies in their sample could be described by homologous spherical Hernquist distributions. These models ignore possible systematic variations of galaxy morphology with mass (e.g. Caon et al. 1993; Kormendy et al. 2009). Moreover real early-type galaxies, even in the mass range of the SLACS survey, are dominated by fast rotating disks (Paper II, Paper III), some of which are clearly visible in the SLACS photometry. Disk galaxies are not well described by spherical single-component models. It is unclear whether galaxy models that do not reproduce neither the kinematics nor the photometry of the real galaxies under study can be trusted at the $\sim$10% level that is required for IMF studies. Possible systematic biases in the results are however difficult to estimate. A reanalysis of the excellent SLACS dataset using more realistic and flexible models would seem the best way to clarify the situation and provide a consistent picture. This approach has already been demonstrated by Barnabè et al. (2012) for a single galaxy using the JAM method (Cappellari 2008) in combination with the lensing analysis. One should finally consider that lensing studies measure the mass wihin cylinders along the line-of-sight. The recovered stellar mass depends on both the assumed dark matter profile in the center, as well as at large radii (Dutton et al. 2011a).

An simple assumption on the dark matter content of early-type galaxies was made by Dutton et al. (2012b). They selected the most dense galaxies from a large sample of SDSS galaxies and constructed spherical isotropic models to reproduce their stellar velocity dispersion. They assumed the total dynamical M/L of this set of galaxies is the same as the stellar one. Comparing the inferred mass to the one from stellar population they concluded the galaxies require on average a Salpeter IMF normalization. This study still depends on the spherical approximation. Moreover it is unclear to what accuracy the zero dark matter assumption is verified even for the densest galaxies. Nonetheless this study confirms that, unlike spiral galaxies, the densest early-type galaxies are not inconsistent with a Salpeter IMF.

In summary, the two result on which nearly all previously discussed studies agree are: (i) the *total* M/L in the central regions of galaxies ($r \lesssim R_{\rm e}$) does not follow the M/L inferred assuming a universal IMF; (ii) less massive galaxies, especially spiral ones, *require* and IMF normalization lighter thank Salpeter and consistent

with Kroupa-like, while more massive and dense ones allow for a Salpeter IMF. Indications were found for the Salpeter IMF to be actually *required* for massive ellipticals (Grillo et al. 2009; Treu et al. 2010; Auger et al. 2010b; Dutton et al. 2012b). However these conclusions depend on assuming the knowledge of either the dark matter fraction or the slope, or the mass of the dark halo. An exception is the recent work by Sonnenfeld et al. (2012), which modelled a rare elliptical with two concentric Einstein rings, and concluded for a Salpeter IMF. More similar objects would be needed to draw solid conclusions. Not all studies agreed on the requirement for a Salpeter IMF, even when analysing the same SLACS data (Ferreras et al. 2008; Tortora et al. 2010; Barnabè et al. 2011; Deason et al. 2012). It seems that this situation could be resolved by the use of more realistic models.

4.1.5 Systematic IMF variation in galaxies

A breakthrough in IMF studies was provided by the work by van Dokkum & Conroy (2010), further strengthened in van Dokkum & Conroy (2011). Contrary to the previously described set of dynamical and lensing works, they looked for evidences of IMF variation in subtle IMF-sensitive spectral features of the near-infrared region of galaxy spectra, in particular the Wing-Ford band. In this way their study did not suffer from the dependency on the halo assumptions. Although the spectral technique has been around for decades (e.g. Spinrad & Taylor 1971), only the availability of reliable stellar population models has made the approach sufficiently accurate for IMF studies (Schiavon et al. 2000; Cenarro et al. 2003). van Dokkum & Conroy (2010) analysed the IMF of eight massive ellipticals, from stacked spectra. They used new population models that allow for a variation of the detailed abundance patterns of the stars (Conroy & van Dokkum 2012a) to distinguish abundance from IMF variations. They concluded that the observed spectra required a bottom-heavy, dwarf-rich IMF. Combining their finding with the previous results on the IMF of spiral galaxies they tentatively concluded that "Taken at face value, our results imply that the form of the IMF is not universal but depends on the prevailing physical conditions: Kroupa-like in quiet, star-forming disks and dwarf-rich in the progenitors of massive elliptical galaxies".

Our relatively large and well-selected ATLAS^{3D} sample and high-quality integral-field stellar kinematics appeared well suited to resolve the halo degeneracies of previous dynamical and lensing analyses and test the claims from the spectral analysis. Contrary to previous large studies, we adopted an axisymmetric modelling method which describes in detail both the individual galaxy images using the MGE technique (Emsellem et al. 1994; Cappellari 2002) and the richness of our two-dimensional kinematics (Cappellari 2008), thus avoiding the possible biases of previous more approximate approaches. For the first time, thanks to the tighter constraints to the models provided by the two-dimensional data, our study could leave *both* the halo slope and its mass as free parameters. The halo slope is allowed to vary in a range which includes both the flat inner halos predicted by halo expansion models (e.g. Governato et al. 2010), and the steep ones predicted by adiabatic halo contraction (Gnedin et al. 2004, e.g.). Our models also explicitly include the galaxy inclination and anisotropy as free parameters, although the latter is still assumed to be constant in the region where we have data. The parameters are estimated in a Bayesian framework with a maximum ignorance (flat) prior on the parameters.

We showed that even in this relatively general case the models required a variation of the IMF to reproduce the data (Cappellari et al. 2012). We additionally tested a variety of sensible modelling assumptions on the halo, some of which had already been employed by previous studies. However this time our models accurately described the photometry and kinematics of the real galaxies. We confirmed that a non-universal IMF is required under all those halo assumption. The similarity is due to the fact that in all cases dark matter contributes just about 10-20% to the total mass within $1R_{\rm e}$, so that it cannot explain an observed M/L excess of up to a factor 2-3.

Our ATLAS^{3D} sample includes a larger range of masses than previous lensing studies. Not only we could quantify the IMF normalization of early-type galaxies as a class, but we showed that the IMF normalization varies systematically within the early-type galaxy population, as a function of the stellar $(M/L)_{\rm stars}$. The IMF was found consistent with Kroupa/Chabrier-like at low $(M/L)_{\rm stars}$ and heavier that Salpeter at large $(M/L)_{\rm stars}$. This finding bridges the gap between the Kroupa-like IMF determinations in spirals and the evidence for a Salpeter-like or heavier in early-type galaxies. This should be expected given the parallelism and continuity in physical parameters between early-type and spiral galaxies as emphasized in our 'comb' morphological diagram (Paper VII). Early-type galaxies at low $(M/L)_{\rm stars}$ in fact completely overlap with the region populated by spiral galaxies on the mass-size projection of the Virial Plane (Fig. 5). Our result also reconciled the apparent disagreement between studies claiming that early-type galaxies include cases with Kroupa/Chabrier normalization and those claiming that Salpeter is required.

Although, unsurprisingly, the cleanest IMF trend in Cappellari et al. (2012) was obtained by simply comparing the dynamical and population M/L, a trend with velocity dispersion σ_e was also presented. This is a natural consequence of existence of the $M/L - \sigma$ correlation (Cappellari et al. 2006; van der Marel & van Dokkum 2007). In particular Cappellari et al. (2012) (their fig. 2) showed an IMF trend, with significant scatter, going from a Kroupa/Chabrier to a Salpeter IMF within the range $\log_{10}(\sigma_e/\mathrm{km\ s^{-1}}) \approx 1.9 - 2.4$, with a gradual variation in between.

A flurry of papers have appeared in subsequent months from independent groups, all in agreement on the existence of a systematic IMF variation in galaxies. Spiniello et al. (2012) used the models of Conroy & van Dokkum (2012a) in combination with SDSS spectra and inferred a variation of the IMF from sodium and titanium-oxide absorptions, which correlate with velocity dispersion (also illustrated by Zhu et al. 2010). A similar result was inferred by Ferreras et al. (2012), also from SDSS spectra, but using the population models by Vazdekis et al. (2012). Smith et al. (2012) studied the Wing-Ford absorption for galaxies in the Coma Cluster. They find that their galaxy spectra are best reproduced by a Salpeter IMF and detect a weak IMF trend with metallicity, but do not find an IMF trend with velocity dispersion. Conroy & van Dokkum (2012b) detected a systematic trend of the IMF, versus either σ or metallicity, using both optical and near-infrared spectral features. A key difference from other spectral studies is that they were able to rule out, in a Bayesian framework, a variation of element abundances as the origin of the empirical trends.

Dutton et al. (2012a) showed that it is sufficient to assume the knowledge of the halo mass and fit galaxy scaling relations via approximate spherical galaxy models, to infer a systematic variation of the IMF. Similarly Tortora et al. (2012) tested a set of different assumption on the dark halo, using approximate spherical Sersic (1968) galaxy models to fit the SDSS velocity dispersion of a large

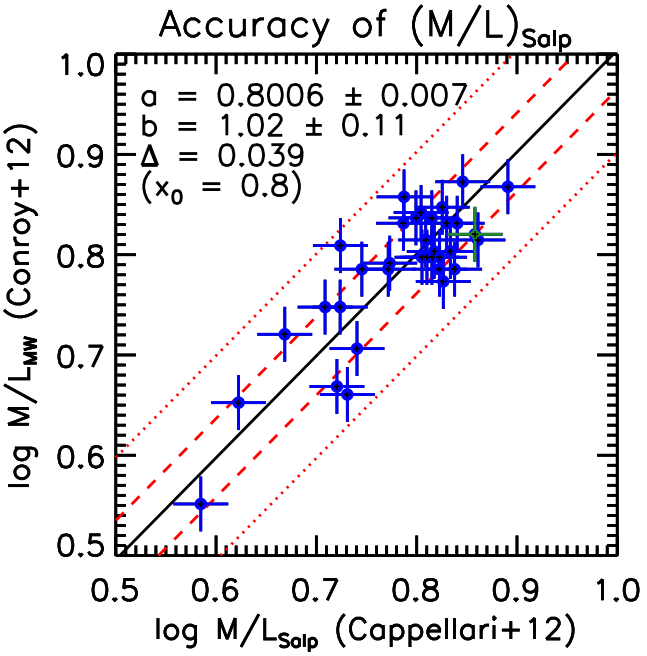

Figure 6. Testing the accuracy of $(M/L)_{\rm Salp}$ against the completely independent determination of Conroy & van Dokkum (2012b),which use a different population code and different spectra with a longer wavelength range than the SAURON ones. Assuming all measurements have comparable errors, the observed scatter between the 35 values is consistent with an error of 6.5% in $(M/L)_{\rm Salp}$.

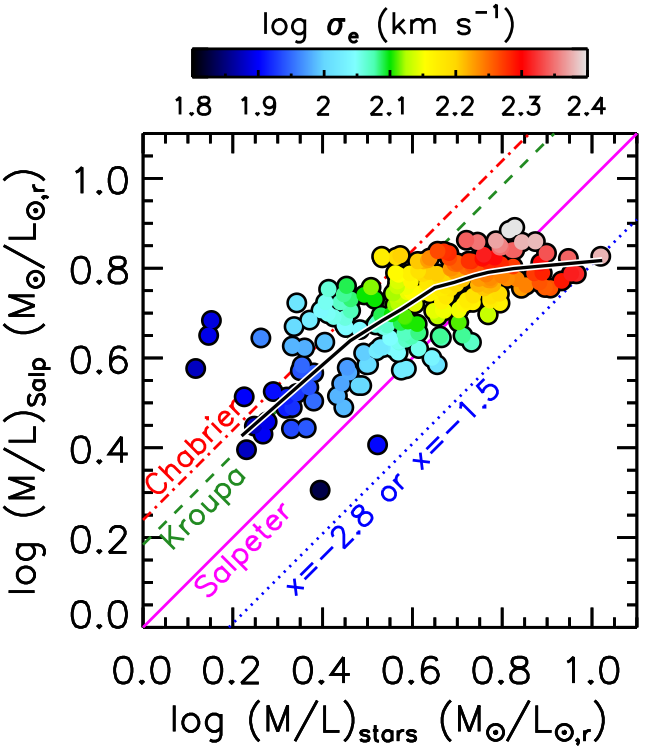

Figure 7. The systematic variation of the IMF. The $(M/L)_{\rm stars}$ of the stellar component, determined via dynamical models, is compared to the $(M/L)_{\rm Salp}$ determined from spectral fitting using stellar population models and assuming for reference a fixed Salpeter IMF. The colours of the symbols show the galaxies σ_e, which was LOESS smoothed in two-dimension to emphasize the trends. Diagonal lines illustrate the expected trends if the IMF was universal or either the Chabrier (red dash-dotted line), Kroupa (green dashed line) or Salpeter ($\zeta(m) \propto m^{-2.3}$, solid magenta line) forms. Also shown is the expected trend for two IMFs heavier than Salpeter (blue dotted line): a top-heavy one, dominated by stellar remnants ($\zeta(m) \propto m^{-1.5}$), and a bottom-heavy one, dominated by dwarfs ($\zeta(m) \propto m^{-2.8}$). The black solid curve is a LOESS smoothed version of the data. A clear systematic trend is evident, with the IMF being closer to Kroupa/Chabrier at the lowest M/L, which also have the lowest σ_e, and closer to Salpeter or heavier at the largest M/L or largest σ_e. A different rendition of this figure was presented in fig. 2b of Cappellari et al. (2012).

galaxy sample. Some of the halo assumptions were also included in Cappellari et al. (2012) with more detailed dynamical models, producing consistent results. Although these results still depend on simple approximations and on assumption on the halo, they illustrate that many different halo assumptions, motivated by theoretical models, all lead to the same conclusion of a systematic IMF variation.

In summary, after years of debate on whether the IMF or the dark matter were responsible for the observed disagreement between stellar population and dynamical or lensing indicators, a consensus seems to have emerged, from dynamical, lensing and spectral arguments, on a systematic IMF variation with the IMF becoming heavier with M/L, mass or velocity dispersion. It is time to investigate IMF trends against other observables, which we do in the following section.

4.2 IMF variation on the Virial Plane

In Cappellari et al. (2012) we presented a systematic trend between the IMF and the stellar $(M/L)_{\rm stars}$ derived using axisymmetric JAM models including a dark halo. The IMF was parametrised by the IMF mismatch parameter $\alpha \equiv (M/L)_{\rm stars}/(M/L)_{\rm Salp}$ (in the notation of Treu et al. 2010), where $(M/L)_{\rm Salp}$ was derived from full spectral fitting as summarized in Section 2.3. Different population approaches were also tested there, producing less clean trends but consistent results. The $(M/L)_{\rm Salp}$ normalization depends on the adopted lower and upper mass cut-offs for the IMF in the population models. The models we use (Vazdekis et al. 2010) adopt standard lower and upper mass cut-offs for the IMF of 0.1 and 100 $M_\odot$, respectively. $(M/L)_{\rm Salp}$ further depends on whether the gas lost by the stars during the early stages of their evolution is retained in the central regions we observe or is recycled into stars or expelled at large radii. Evidence suggests the gas is not retained in significant quantities within $1R_{\rm e}$, neither in ionized or hot X-ray emission form (Sarzi et al. 2010), nor as a cold component (Young et al. 2011, hereafter Paper IV). If all the gas was retained it would increase $(M/L)_{\rm Salp}$ by up to 30–40% (Maraston 2005), making population M/L overpredicting total dynamical M/L even for a light Kroupa/Chabrier IMF, for a number of galaxies.

A careful determination of the population M/L for a fixed IMF was recently provided for 35 galaxies in our sample by Conroy & van Dokkum (2012b). They employed different models (Conroy & van Dokkum 2012a) from the ones we adopted (Vazdekis et al. 2010) and used them to fit an independent set of spectra, spanning a larger wavelength range than the SAURON ones. In Fig. 6 we compare the two determinations of M/L (allowing for an arbitrary offset in the absolute normalization, which can differ by up to 10% between different authors). Assuming all measurements have comparable errors, the observed scatter between the 35 values is consistent with an error of just 6.5% in $(M/L)_{\rm Salp}$. This

error is consistent with the error of 7% predicted by Gallazzi & Bell (2009) when optimal spectra information is available. This gives confidence that our population $(M/L)_{\rm Salp}$ are robust and any trend we observe is not due to the details of our population modelling approach.

Cappellari et al. (2012) showed that consistent IMF trends are found for a variety of different assumptions on the dark halo, as well as for the most general one (with gNFW halo) that leaves both the halo slope and mass as free parameters, with only an upper limit on the halo slope, derived from model predictions of halo contraction (Gnedin et al. 2011) (see Paper XIX). The similarity in $(M/L)_{\rm stars}$ for the different models is due to the fact that in all cases the data allow for a small fraction of dark matter within the region where the kinematics are available ($\sim$1$R_{\rm e}$), with the most general model implying a median dark matter fractions of just 10%. Given the similarity of the different approaches, here we adopt as reference the $(M/L)_{\rm stars}$ values obtained with a NFW halo, with halo mass as free parameter (model (B)). This choice makes it easy to compare our results with others that make the same assumption.

In Fig. 7 we show a different rendition of the similar fig. 2b of Cappellari et al. (2012). Here we plot $(M/L)_{\rm Salp}$ versus $(M/L)_{\rm stars}$. We still exclude galaxies with very young stellar populations, selected as having stellar absorption line strength index H$\beta > 2.3$ Å. We found that those galaxies have strong gradient in the stellar population and this breaks our approximate assumption of a constant $(M/L)_{\rm stars}$ within the region where we have kinematics, making both $(M/L)_{\rm stars}$ and $(M/L)_{\rm Salp}$ inaccurate and ill-defined. Different diagonal lines illustrate the expected trends if the IMF was universal or either the Chabrier, Kroupa or Salpeter ($\zeta(m) \propto m^{-2.3}$) forms. Also shown is the expected trend for two IMFs heavier than Salpeter: a top-heavy one, dominated by stellar remnants ($\zeta(m) \propto m^{-1.5}$), and a bottom-heavy one, dominated by dwarfs ($\zeta(m) \propto m^{-2.8}$). This figure clearly illustrates the fact that the two indicators of M/L do not follow a one-to-one relation, but deviate systematically, with the IMF being consistent on average with Kroupa/Chabrier at the lowest $(M/L)_{\rm stars}$ and with Salpeter or heavier at the largest $(M/L)_{\rm stars}$, as already concluded in Cappellari et al. (2012). Another way to interpret this plot is by noting that galaxies with the largest $(M/L)_{\rm Salp}$, which are characterized by the oldest populations, have a Salpeter or heavier IMF, while those with the lowest $(M/L)_{\rm Salp}$, which have younger populations, have on average a Kroupa/Chabrier IMF. Detailed trends of the IMF with other population indicators will be presented in McDermid et al. (in preparation).

As in the Cappellari et al. (2012) we also show with colours the galaxies velocity dispersion. However, to emphasize the trend, here we apply the same two-dimensional LOESS smoothing approach (Cleveland & Devlin 1988) introduced in Section 3, instead of showing the individual σ_e values. One can still see the trend for the IMF to vary between Kroupa/Chabrier to Salpeter, albeit with large scatter, within the interval $\log_{10}(\sigma_e/{\rm km\ s^{-1}}) \approx 1.9 - 2.4$, with a smooth variation in between. This trend will be more precisely quantified in Section 4.3.

In Fig. 8 we show the variation of the IMF mismatch parameter $(M/L)_{\rm stars}/(M/L)_{\rm Salp}$ on the (M, σ_e) and $(M, R_{\rm e})$ projections of the Virial Plane. The trends in IMF are necessarily noisier that the ones in $(M/L)_{\rm stars}$, as here the errors in both M/L combine. However the structure in this figure closely resembles the one in the previous Fig. 1, 2 and the top panel of Fig. 3. The systematic variation in the IMF follows on average the variations in the total $(M/L)_{\rm JAM}$ and its corresponding stellar population indicators Hβ and galaxy colour. Like the other quantities, also the IMF appears to roughly follow lines of constant σ_e on the Virial Plane, which we showed is tracing the bulge mass at given galaxy size and mass. In both projections there is indication for some extra substructure, with IMF variation at constant σ_e. Moreover the proximity to the ZOE (thick red line) seems to be an even better indicator of IMF than σ_e (blue dashed lines). The $(M, R_{\rm e})$ projection also makes clear why one should expect spirals to have on average light IMF: spirals populate the empty zone above our galaxies (Fig. 5 and fig. 4 in Paper I) and overlap with the distribution of ETGs with the Kroupa/Chabrier IMF. However our plot suggests that, at fixed galaxy stellar (or $M_{\rm JAM}$) mass, the bulge mass (as traced by σ_e) is the main driver of the IMF variation, rather than morphological type alone, and one may expect IMF variations within the spiral population as well. Our finding explains why Dutton et al. (2012b) inferred a Salpeter or heavier IMF when selecting the smallest (or densest) galaxies at fixed mass, and assuming no dark matter. Dark matter appears to provide a small contribution to the M/L for our entire sample and not just the smallest ones, but the densest galaxies are precisely the ones with the heaviest IMF. A recent claims has been made for a Salpeter IMF in the bulge of 5 massive spirals (Dutton et al. 2012c), which would go in the suggested direction. However the IMF is currently already difficult to infer when the M/L can be assumed to be spatially constant and the stellar population homogeneous. Relaxing these assumptions makes the results more uncertain unless very good population data from galaxy spectra and accurate non-parametric models for the photometry are employed.

4.3 IMF versus σ_e correlation

In the previous section we illustrated the systematic IMF trends already presented in Cappellari et al. (2012) and we additionally presented the variation of the IMF on the projections of the Virial Plane. We pointed out that, like the dynamical M/L, its population indicators, colour and Hβ, and the galaxy concentration which traces to the bulge mass, also the IMF broadly follows lines of nearly constant σ_e on the $(M_{\rm JAM}, \sigma_e)$ Virial Plane projection and consequently constant $\sqrt{GM_{\rm JAM}/(5R_{\rm e}^{\rm max})} \approx \sigma_e$ on the $(M_{\rm JAM}, R_e^{\rm max})$ projection. Interestingly a 'conspiracy' between the IMF variation and other galaxies properties is required for galaxy scaling relations to still have a small scatter (Renzini & Ciotti 1993).

In Fig. 9 we present a direct correlation between the logarithm of the IMF mismatch parameter $(M/L)_{\rm stars}/(M/L)_{\rm Salp}$ and the logarithm of σ_e, using the robust linear fitting routine LTS_LINEFIT presented in (Paper XIX), which explicitly allows and fits for intrinsic scatter and removes outliers. Like earlier we exclude galaxies with very young stellar populations, selected s having stellar absorption line strength index H$\beta > 2.3$ Å, leading to a sample of 223 out of 260 galaxies. In the fits we quadratically coadded JAM modelling errors of 6% (Paper XIX) plus distance errors for $(M/L)_{\rm stars}$, population models errors of 6.5% for $(M/L)_{\rm Salp}$ (Fig. 6) and 10% for our photometry Paper XXI. We present fits for (i) the full sample, (ii) for the subsample of galaxies with SBF distances (mostly from Tonry et al. 2001 and Mei et al. 2007: see Paper I) and (iii) for galaxies with $\sigma_e > 90$ km s^{-1}, to eliminate a few objects with larger scatter. All three relations have a comparable observed scatter $\Delta \approx 0.10$ dex (26%) in $(M/L)_{\rm stars}/(M/L)_{\rm Salp}$ and imply a significant intrinsic scatter of about 20%. When the same outliers are removed, we verified that indistinguishable values for the parameter, their errors and the infered intrinsic scatter are obtained with the Bayesian approach of Kelly (2007), as im-

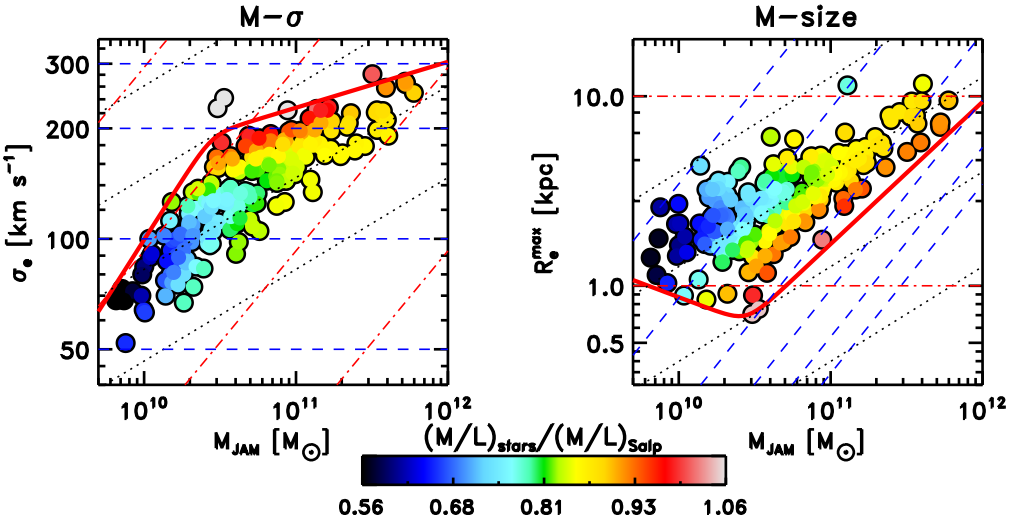

Figure 8. Variation of the IMF on the Virial Plane projections. Same as in Fig. 1 for the variation of the IMF mismatch parameter $(M/L)_{\rm stars}/(M/L)_{\rm Salp}$, which measure the ratio between the stellar M/L from dynamical models and the one from population models, with a fixed Salpeter IMF for reference. The trends follow lines of roughly constant σ_e, or perhaps depends on the distance from the ZOE (thick red line), although some extra structure is visible.

plemented in his IDL routine LINMIX_ERR. Our three fits provide consistent values for the best-fitting slopes, within the errors, and nearly consistent normalizations. The fitted relation has the form

$$\log_{10}\frac{(M/L)_{\rm stars}}{(M/L)_{\rm Salp}} = a + b\times\log_{10}\frac{\sigma_e}{130{\rm km\ s^{-1}}}, \qquad (6)$$

and our preferred values (bottom panel of Fig. 9) have best fitting parameters and formal errors $a = -0.11\pm0.01$ and $b = 0.36\pm0.06$ (parameters and errors for the other fits are given inside the figures). The observed trend of IMF with σ appears to account for about half of the total trend in the $(M/L)-\sigma_e$ relation $(M/L)_{\rm JAM}\propto\sigma_e^{0.62}$ (see Paper XIX), the remaining one being due to stellar population variations.

Our trend implies a transition of the mean IMF from Kroupa to Salpeter in the interval $\log_{10}(\sigma_e/{\rm km\ s^{-1}})\approx 1.9-2.4$ (or $\sigma_e\approx 80-260$ km s^{-1}), with a smooth variation in between, consistently with what can be seen in Cappellari et al. (2012) and in Fig. 7. The fact that this trend is slightly weaker than the one implied by Fig. 7 seems to confirms the intrinsic differences in the IMF of individual galaxies. However, part of this difference could also be explained if the distance errors were underestimated. One way to address this issue would be to repeat our analysis for galaxies in a clusters at intermediate distance like the Coma cluster, for which relative distance errors can be neglected.

Our slope is a factor ≈ 3.6 smaller than the "tentative" trend reported in Treu et al. (2010) for the same quantities, and making the same assumption for the dark halo. A reason for this large difference must be due to the fact that their sample only included galaxies with $\sigma\gtrsim 200$ km s^{-1} ($\log_{10}(\sigma/{\rm km\ s^{-1}})\gtrsim 2.3$). Our sample is too small to reliably study trend in IMF for the galaxies above that σ_e, but their reported trend would exceed the slope of the $(M/L)-\sigma$ relation (Paper XIX), making it difficult to explain. Their steep inferred trend may then be due to their use of spherical and homologous models for all the galaxies, which may introduce systematic trends. Moreover they used single stellar population M/L based on colours is expected to be less reliable than our determinations based on spectra (Gallazzi & Bell 2009). A reanalysis of the unique SLACS dataset seems required to clarify this issue. Our trend with σ_e is also smaller than the one reported by Ferreras et al. (2012) from spectral analysis, who find a rapid change from a Kroupa to a Salpeter IMF in the narrow interval $\sigma\approx 150-200$ km s^{-1}. Our relation is not inconsistent with the values presented in Conroy & van Dokkum (2012b) also from spectral analysis, or with the result reported by Spiniello et al. (2012), with the IMF becoming steeper than Salpeter above $\sigma\gtrsim 200$ km s^{-1}. We are also broadly consistent with the IMF variation implied by the non-contracted halo spherical dynamical models of Tortora et al. (2012). Overall there is a qualitative agreement between different approaches and the still significant systematic differences in the various methods could account for the differences.

5 DISCUSSION

5.1 Previous relations as seen on the Virial Plane

We have shown in Paper XVII that galaxy scaling relation can be accurately explained by simple virial equilibrium, with galaxies lying on a tight Virial Plane $(M_{\rm JAM}, \sigma_e, R_e^{\rm maj})$, for a large volume-limited sample of ETGs (Paper I). Once this has been established, the interesting information on galaxy formation is then all contained in the distribution and the physical properties of galaxies on this plane, which we presented in this paper.

We find that on the VP: (i) galaxies sizes are delimited by a lower-boundary, which has a minimum at a characteristic mass $M_{\rm JAM}\approx 3\times10^{10}M_\odot$; (ii) A number of key galaxy properties: dynamical M/L, and its population indicators Hβ and colour, which are mainly related to age (Cappellari et al. 2006), the normalization of the IMF and the prominence of the bulge, all tend to be constant along lines of constant σ_e, on the Virial Plane; (iii) Another characteristic mass for galaxy properties is the value $M_{\rm JAM}\approx 2\times10^{11}M_\odot$ which separates a region dominated by the round or weakly triaxial slow rotators at large masses from one dominated dominated by fast-rotators ETGs, flattened in their outer parts and with embedded exponential disks (Paper XVII), whose characteristics merge smoothly with the ones of spiral galaxies. A transition at this galaxy mass appears required in our models for the formation of fast and slow rotators (Khochfar et al. 2011, hereafter Paper VIII). Interestingly the approximate stellar mass

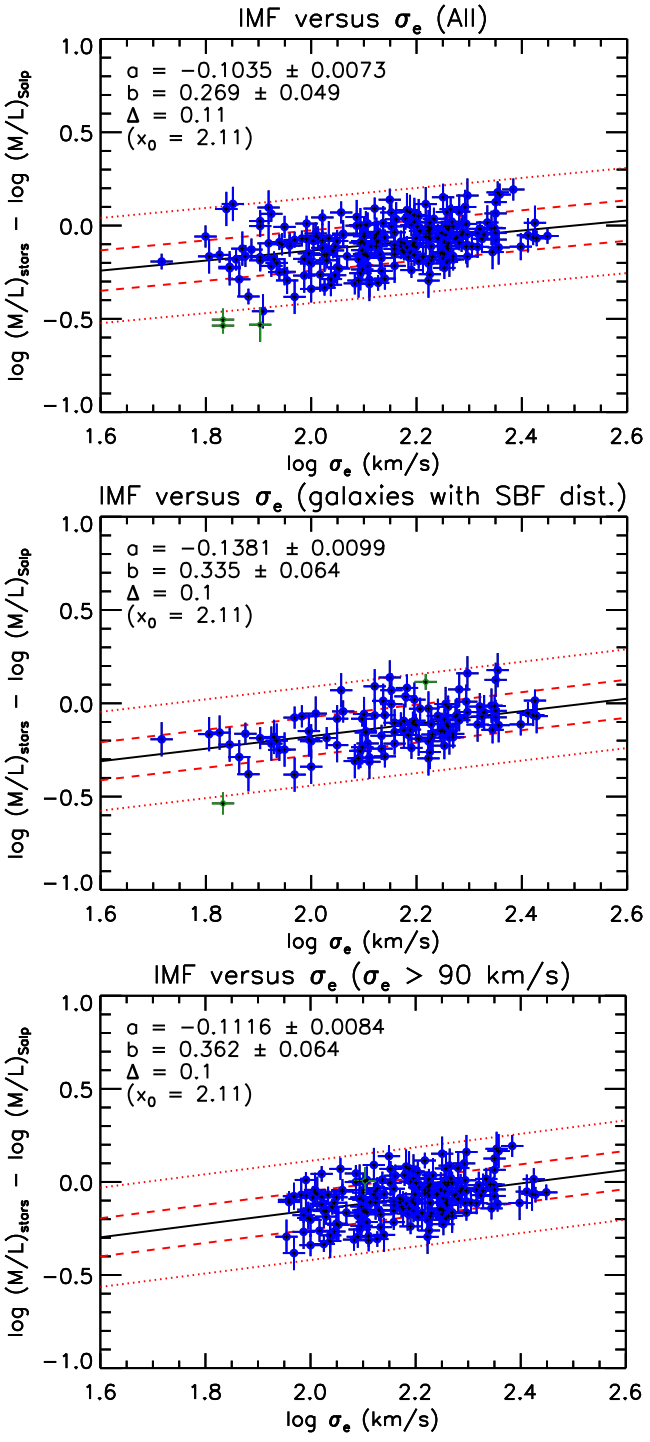

Figure 9. IMF versus σ_e correlations. The plots show as blue filled circles with error bars the logarithm of the IMF mismatch parameter $(M/L)_{\rm stars}/(M/L)_{\rm Salp}$ versus the effective velocity dispersion σ_e, for the subsets of 223 ATLAS^{3D} galaxies with H$\beta > 2.3$ Å. Green symbols are outliers automatically removed from the fits. Dashed and dotted red lines indicate the 1σ and 2.6σ (99%) observed scatter around the best-fitting relation (black solid line). The top panel includes all 223 galaxies. The middle panel shows galaxies with accurate SBF distances. The bottom panel shows galaxies with $\sigma_e > 90$ km s^{-1}.

$M_\star \approx 1 \times 10^9\ M_\odot$ where normal early-type galaxies starts to appear corresponds to the threshold for quenching of field galaxies recently discovered by Geha et al. (2012). Below that mass only the cluster or group environment can strip spirals of their gas.

Although our sample is limited to a minimum mass $M_{\rm JAM} \gtrsim 6 \times 10^9\ M_\odot$, our picture extends smoothly to lower masses. A comparison of the trends outlined in fig. 4 of Paper I or Fig. 5 here, with similar relations for lower mass galaxies (e.g. fig. 7 of Binggeli et al. 1984; fig. 38 of Kormendy et al. 2009; fig. 12 of Chen et al. 2010; fig. 4 of Misgeld & Hilker 2011; fig. 20 of Kormendy & Bender 2012) clearly shows that our ETGs trends continues with the dwarf spheroidal (Sph) sequence at lower masses, while the spirals sequence continues with a sequence of low-mass late spirals or irregulars (Sc–Irr), as independently noted also by Kormendy & Bender (2012). The parallelism between ETGs and spiral galaxies in scaling relations was one of the driver for our proposed revision (Paper VII) to the tuning-fork diagram by Hubble (1936), in the spirit of van den Bergh (1976). In Fig. 10. we combine our results on morphology, kinematics and scaling relations in a single diagram, using the same galaxy symbols as Paper VII. This picture allows us to provide a new perspective and a clean empirical view of a number of classic scaling relation and known trends in galaxy properties.

The classic Faber & Jackson (1976) relation between $\sigma - L$ is well known to be a projection of the FP. We study it here using mass instead of light, and find that it is tracing the envelope defined by the ZOE. We find that the relation is not well described by an approximately linear trend. This is consistent with some earlier claims of a possible change in the slope of the $\sigma - L$ relation of elliptical galaxies at the low luminosity end (Tonry 1981; Davies et al. 1983; Tortora et al. 2009). However even recent observations from the large SDSS sample have subsequently failed to find evidence for a clear curvature, likely due to the insufficient quality of the data (Bernardi et al. 2003; Gallazzi et al. 2006). For this reason the relation is generally assumed to be a power-law, except in the region of dwarf ellipticals (de Rijcke et al. 2005; Matković & Guzmán 2005; Forbes et al. 2008; Cody et al. 2009). The reason for this confusion is that the $(M_{\rm JAM}, \sigma)$ projection is not too far from an edge-on view so that the bend in the ZOE is not well pronounced and the evidence for the bend can be robustly detected here for the first time in ETGs. Samples of morphologically selected elliptical galaxies, for which the relation is usually derived, tend to populate mainly the top (red) region of the diagram, where the effect of the cusp is not evident. Moreover most previous studies did not reliably sample the lowest σ regime.

Another well known projection of the FP is the Kormendy (1977) relation. When using mass instead of light it becomes clear it represents the analogue of the Faber & Jackson (1976), but this time in the $(M_{\rm JAM}, R_e^{\rm max})$ projection of the VP. Also in this case, when samples are morphologically selected to consist of ellipticals, they tend to populate mostly the region of the diagram near the ZOE, defining a relatively narrow sequence (Kormendy et al. 2009; Chen et al. 2010; Misgeld & Hilker 2011). Although the sequence is useful for a number of studies, it is important to realize that it is not a real sequence in galaxy space on the VP. It is due to the sample selection and it represents essentially one of the contour levels of a continuous trend of galaxy properties, spanning from spiral galaxies, to ETGs, and only terminating on the well defined ZOE (Fig. 5 and figure 4 in Paper I).

The characteristic mass $M_{\rm JAM} \approx 3 \times 10^{10} M_\odot$ is the same transition mass discovered by Kauffmann et al. (2003a) who state that "low-redshift galaxies divide into two distinct families at a stel-

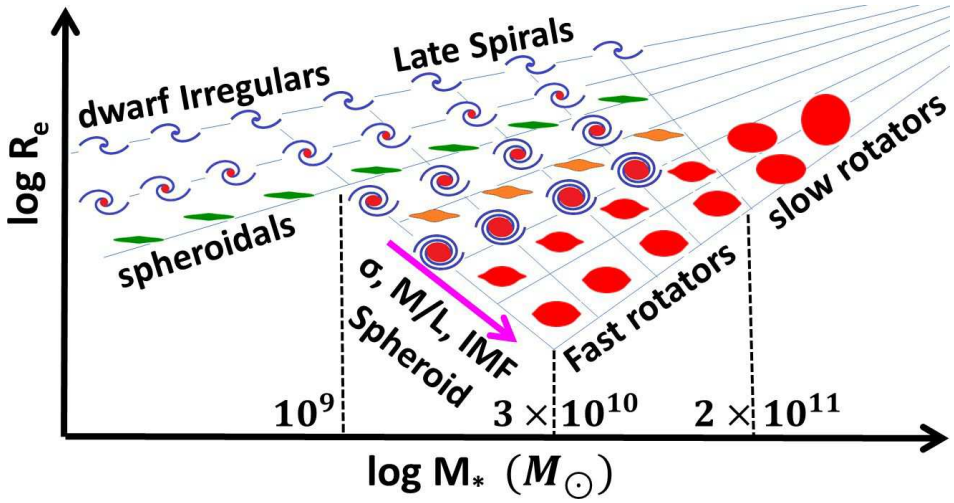

Figure 10. Schematic summary of the results presented in Section 3 and Section 4. ETGs properties, dynamical M/L (Fig. 1) or its population proxies, Hβ and galaxy colour (Fig. 2), concentration (Fig. 3), which traces bulge mass, and IMF mass normalization (Fig. 8), all tend to vary along lines of nearly constant $\sqrt{GM_\star/(5R_{\rm e}^{\rm max})} \approx \sigma_e$. This sequence of ETGs properties merges smoothly with the one of spiral galaxies, with little overlap between late spirals (Sc-Irr) and ETGs, a significant overlap between early spirals (Sa-Sb) and fast-rotator ETGs with low M/L and no overlaps between spirals and fast-rotators with high M/L. Three characteristic masses are emphasized in this diagram: (i) below $M_\star \approx 10^9\ M_\odot$ there are no regular ETGs and the mass-size lower boundary is increasing; (ii) $M_\star \approx 3\times10^10\ M_\odot$ is the mass at which ETGs reach their minimum size (or maximum stellar density), before a sudden change in slope $R_{\rm e} \propto M^{0.75}$ at larger masses (see also fig. 4 in Paper I); (iii) Below $M_\star \approx 2\times10^{11}\ M_\odot$ ETGs are dominated by flat fast rotators, showing evidence for disks (Paper XVII), while slow rotators are rare. Above this mass the population is dominated by round or weakly triaxial slow rotators. These smooth trends in scaling relations motivated our proposed parallelism between spirals and ETGs. To emphasize this connection we uses the same morphology symbols as our 'comb' diagram in Paper VII.

lar mass of $3\times10^{10}M_\odot$. Lower-mass galaxies have young stellar populations, low surface mass densities and the low concentrations typical of discs. Their star formation histories are more strongly correlated with surface mass density than with stellar mass." A similar trend involving colours and also better correlated with surface density (or with the velocity dispersion inferred from the scalar virial relation) than with mass, was found to extend to redshift up to $z \approx 3$, with red galaxies being systematically small, and blue galaxies being large at a given mass (Franx et al. 2008). This was recently confirmed, still using photometric data alone, by Bell et al. (2012). The correctness of all these statements can now be easily and accurately verified for the ETGs subset in Fig. 1–3.

The novelty of our work, with respect to all previous studies, is that we have unprecedentedly accurate and unbiased dynamical masses, and stellar velocity dispersions, instead of inferred value. This allow us to conclusively state that neither dynamical mass nor stellar surface density are actually the best descriptor of galaxy properties, the main trend being along the σ_e direction (which includes rotation in the case of disk galaxies). Our clean ATLAS$^{\rm 3D}$ result was already presented in Cappellari (2011a) and subsequently confirmed with SDSS data and using virial mass estimates by Wake et al. (2012). The trend we observed for the ETGs can be extended to spiral galaxies, which fill the region of larger sizes above the ETGs in the $(M_{\rm JAM}, R_e^{\rm max})$ projection, smoothly overlapping with the ETGs for the largest spiral bulge fractions (figure 4 of Paper I and Fig. 5). It has been known for long that in spirals luminosity-weighted ages are lower, star formation is larger and colours bluer on average than the ETGs, essentially by definition (e.g. Hubble 1936; van den Bergh 1976).

Similar trends between age and size (or surface brightness), with older objects being smaller at given age, were found to persist in ETGs. van der Wel et al. (2009a) state that "at a given stellar velocity dispersion, SDSS data show that there is no relation between size and age". The same age-size trend was pointed out by Shankar & Bernardi (2009), and in different terms by Graves et al. (2009) who state that "no stellar population property shows any dependence on $R_{\rm e}$ at fixed σ, suggesting that σ and not dynamical mass is the better predictor of past SFH". The age-size trend was also confirmed in different samples of galaxies by Valentinuzzi et al. (2010) and Napolitano et al. (2010). All these findings are another way of saying that age variations must follow lines of constant σ on the VP as we find here for M/L, $H\beta$ and colour, and confirm using age for our sample in McDermid et al. (in preparation) (see also figure 15 of Gallazzi et al. 2006). The only contrasting view is the one by Trujillo et al. (2011), who find a lack of age-size trend both at low and high-redshift.

The same characteristics mass $M_{\rm JAM} \approx 3\times10^{10}\ M_\odot$ of Kauffmann et al. (2003a), which constitute the location of the break in our ZOE, was found by Hyde & Bernardi (2009a) in the mass-size relation of 5×10^4 SDSS galaxies, their trend is significant but quite subtle. The reason for the curvature they find becomes clear from what we find: the average radius of the objects on the VP at constant mass, bends upwards at low masses, due to the cusp in the ZOE, with the strength of the effect being dependent on the specific criterion adopted to select ETGs. The bend in the mass-σ however is essentially undetected in the SDSS data, likely due to the insufficient quality of the kinematics, especially at low σ (Hyde & Bernardi 2009a).

A curvature in the luminosity-size relation was presented in Graham & Worley (2008) (see also Chen et al. 2010). It appears when joining dwarf spheroidal galaxies (Sph) and ellipticals as a continuous sequence, with smoothly varying Sersic (1968) index. The observed continuity of the relation is interpreted as a physical connection between dwarf spheroidals and ellipticals. The trend discussed by Graham & Worley (2008) can also be seen in Binggeli et al. (1984), Kormendy (1985), Kormendy et al.

(2009) and Misgeld & Hilker 2011, where the dwarf spheroidals sequence appears to sharply bend from the ellipticals sequence. But Kormendy (1985) interprets dwarf spheroidal as constituting a separate family, of gas-stripped dwarf spirals/irregulars (see Graham 2011 and Kormendy & Bender 2012 for two complementary reviews of this subject).

Our results cannot not be compared to theirs in a statistical sense, as galaxies in their diagrams are, by design, not representative of the population in the nearby Universe, and certain classes of objects (e.g. M32) are by design over-represented. Our sample is volume-limited and for this reason gives a statistically representative view of the galaxy population above a certain mass. Still the fact that the sequence of dwarf spheroidals and low-mass spirals/irregulars, lie on the continuation of our trends for fast rotator ETGs and spiral galaxies respectively, below the $M \lesssim 6 \times 10^9 M_\odot$ mass limit of our survey, suggests a continuity between dwarf spheroidals and the low-mass end of our disk-dominated fast-rotator ETGs population, which in turns we showed are closely related to spiral galaxies. For this reason our results reconciles the apparent contrast between the findings of a Sph-E dichotomy (Kormendy 1985; de Rijcke et al. 2005; Janz & Lisker 2008; Kormendy et al. 2009) and the ones of a continuity (Graham & Guzmán 2003; Gavazzi et al. 2005; Graham & Worley 2008; Forbes et al. 2011). Our finding in fact agrees with the proposed common origin of dwarf spheroidal and low-mass spiral galaxies and irregulars (Kormendy 1985; Dekel & Silk 1986), but also shows an empirical continuity between dwarf spheroidals and a subset of the ellipticals family. The missing link between Sph and E is constituted by disk-dominated fast rotator ETGs (Emsellem et al. 2007; Cappellari et al. 2007). In fact the continuity is not between "true" ellipticals, namely the slow rotator, and dwarf spheroidals, but between "misclassified" ellipticals with disks and S0, namely the fast rotators, and dwarf spheroidals. After this text was written and the parallelism between spiral galaxies and early-type were presented (Paper VII) to interpret the trends we observed in galaxy scaling relations (Paper I and Cappellari 2011a), a confirmation of this picture, including its extension to low mass systems was also provided by Kormendy & Bender (2012).

In summary our view of the VP is consistent and provides a confirmation and the cleanest empirical view of all these reported trends between galaxy properties, which we interpreted as due to the variation of the bulge fraction in fig. 4 of Paper I and explained as due to an apparent conversion of spirals into fast rotators ETGs in Paper VII.

5.2 Implications for galaxy formation

Galaxy formation is the superposition of a number of complex events that happen in parallel. Here we sketch a tentative picture of some of the phenomena that can play a role in explaining what we see. We refer the reader to Bois et al. (2011, hereafter Paper VI), Paper VIII and Naab et al. (in preparation) for a more in-depth discussion.

The smoothness and regularity of the trends we observe and the fact that they extend to spirals, appears to indicate a close connection between the formation of the two classes of objects (Paper VIII). The same similarity between the fast rotator ETGs and spirals in terms of their morphology and degree of rotation, lead us to propose a revision (Paper VII) of the classic morphological classification (Hubble 1936) to emphasize the parallelism between the fast rotators and spirals, in the same way that van den Bergh (1976) proposed it for S0s and spirals. Only the most massive slow rotators appear to form an empirically separated class. The *kinematic* morphology-density relation (Paper VII), which applies to our kinematic classes the relation discovered by Dressler (1980), suggest that most spirals are being transformed into fast rotators due to environmental effects (Khochfar & Ostriker 2008), with a mechanism that is sufficiently 'gentle' to preserve the near axisymmetry of the disk (Paper II).

One process which is often mentioned in the context of cluster galaxy populations is stripping by the interstellar medium (Spitzer & Baade 1951; Abadi et al. 1999), which may impact the global morphology of the galaxy by removing a significant fraction (or most) of its gas content but mostly preserving the stellar disk component. This may explain some of the most flattened galaxies in the fast rotator class (e.g., NGC4762), as emphasised in Paper VII. This would work by removing some of the mass of the galaxy keeping a relatively constant effective size (of the stellar component), and may contribute to the scatter in the Mass-size plane for fast rotator as well as to their overlap with the more gas-rich spiral galaxies.

As to explain the intermediate to high mass end of the fast rotator class, we would need a process which is able to increase the bulge size, while at the same time removing the gas or shutting off star formation (Paper VIII). The empirical signatures of this phenomenon are visible in our data as an 'apparent' decrease of the galaxy size, and increase of σ_e, which is actually due to the bulge concentrating more light at smaller radii, accompanied by a increase in M/L, which is tracing a decrease of star formation or an age increase. The process appears to generally preserve the intrinsic flatness of the stellar disks at large radii (middle panel of Fig. 3). A similar scenario was recently proposed by Bell et al. (2012) to interpret the relationship between rest-frame optical colour, stellar mass, star formation activity, and galaxy structure from $z \approx 2$ to the present day.

Intense gas-rich accretion events, mostly via cold streams (Dekel et al. 2009), or major gas rich mergers (Paper VIII), will increase both the mass and Σ_e. During the accretion the gas may sink toward the centre (Mihos & Hernquist 1994) until it becomes self-gravitating and starts forming stars. It is during this phase of rapid gas accretion that the $M/L - \sigma$ (Cappellari et al. 2006) and IMF $- \sigma$ (Section 4.3) relations, the tilt of the FP (Dressler et al. 1987; Faber et al. 1987; Djorgovski & Davis 1987), the $\mathrm{Mg}b - \sigma$ (Burstein et al. 1988; Bender et al. 1993) or the $\mathrm{Mg}b - V_{\rm esc}$ relation (Davies et al. 1993; Scott et al. 2009, Paper XXI), will be imprinted in the ETGs population (Robertson et al. 2006; Hopkins et al. 2009b) and then mostly preserved in the following evolution.

The early progenitors of today's fast rotator ETGs would be high-redshift spirals, which are different from local ones. They are characterized by giant gas clumps (Elmegreen et al. 2007; Genzel et al. 2011) have high gas fractions (Tacconi et al. 2010; Daddi et al. 2010) and possess large velocity dispersion (Förster Schreiber et al. 2006, 2009; Law et al. 2012). In that situation bulges may form naturally as the clumps collide and may either sink to the centre (Bournaud et al. 2007) or are efficiently destroyed by stellar feedback (Genel et al. 2012; Hopkins et al. 2011). Secular effects (Kormendy & Kennicutt 2004) will also contribute to the bulge growth and Σ_e increase, while keeping the mass unchanged, as will contribute the destabilizing effect of minor mergers.

During the bulge growth some process must be able to turn off star formation, without destroying the fast rotating disks that still dominate the local ETGs population (Paper II; Paper III)

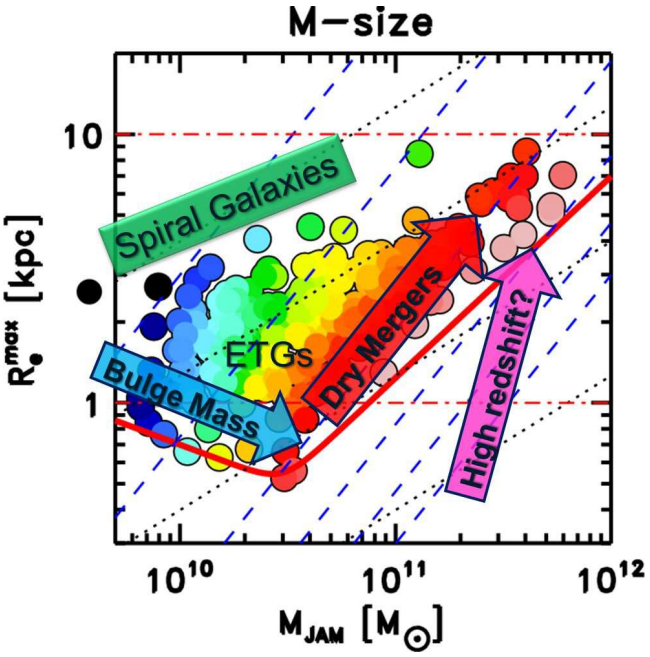

Figure 11. Evolution scenario for ETGs. The symbols are the same as in Fig. 1, while the large arrows indicate the proposed interpretation of the observed distribution as due to a combination of two processes (a) bulge or spheroid growth, which seems associated to the quenching of star formation, which moves galaxies to the right of towards the bottom, due to the increased concentration (decreasing $R_{\rm e}$), and (b) dry merging, increasing $R_{\rm e}$ by moving galaxies along lines of roughly constant σ_e (or steeper), while leaving the population unchanged. A schematic illustration of these two processes is shown in Fig. 12.

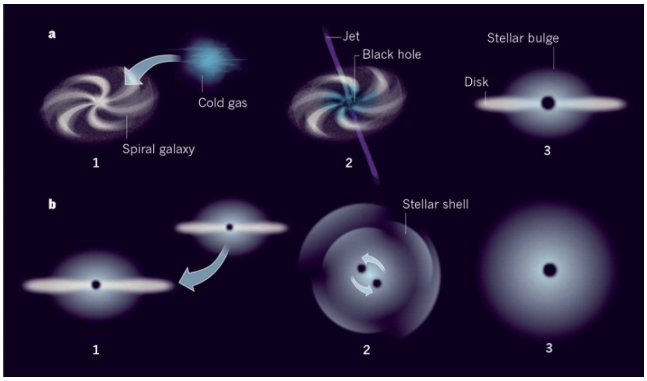

Figure 12. Schematic representation of the two main processes responsible for the formation of the observed distribution of galaxies on the VP. (a) bulge growth via cold accretion, secular evolution, or minor mergers, followed by quenching by AGN or other mechanisms, leaving the galaxy more massive, more compact, and consequently with a larger σ_e, and gas poor (blue arrow in Fig. 11); (b) major or minor dry mergers, increasing galaxy mass and sizes at nearly constant σ_e, or with a possible decrease, leaving the population mostly unchanged (red arrow in Fig. 11). (taken from Cappellari 2011b).

and that dominates the ETGs population already from $z \sim 2$ (van der Wel et al. 2011; see also van Dokkum 2011). The reduced efficiency of star formation by morphological quenching (Martig et al. 2009) may be one of the processes explaining why on average bigger bulges correspond to older ages and larger M/L. But bulge/spheroid growth seems also associated with AGN feedback, which would provide another bulge-related quenching mechanism (Silk & Rees 1998). During the sequence of bulge/spheroid-growth followed by quenching, the original gas rich spiral will move from the left of the observed $(M_{\rm JAM}, R_e^{\rm max})$ plane towards the right, or possibly the bottom right due to the increased concentration, while intersecting the constant σ lines (blue arrow in Fig. 11). At the end of the evens the galaxy will be a fast rotator ETG, generally more massive and with a bigger bulge (smaller $R_{\rm e}$, larger σ_e and concentration) than the precursor clumpy spiral.

At any stage during the bulge-growth phase the galaxy may accrete purely stellar satellites (Khochfar & Silk 2006). In the case of these dry mergers the situation is quite different and one can predict the final configuration using energy conservation (Hernquist et al. 1993; Cole et al. 2000; Boylan-Kolchin et al. 2006; Ciotti et al. 2007). The predictions show that sizes will increase as the mass grows. For major mergers (equal mass) and typical orbital configurations, one can show that the mass and radius double, while σ remains constant in agreement with simulations (Nipoti et al. 2009) (see Hilz et al. 2012b and Hilz et al. 2012a for more accurate numerical simulations and detailed physical explanations of this process). While in the limit in which the same mass doubling happens via small satellites, as mostly expected from the shape of the Schechter (1976) mass function, the radius will increase by a factor of four and the dispersion will be twice smaller (Naab et al. 2009; Bezanson et al. 2009; Hopkins et al. 2009a; Hilz et al. 2012b). As a result the galaxy will move along lines that are parallel to the constant σ lines, or steeper. During these dry mergers, given that there is little gas involved, the stellar population, colour and M/L will remain unchanged (red arrow in Fig. 11).

The gas-rich mergers/accretion scenario is generally consistent with the observed correlation between supermassive black holes (BH) and galaxy velocity dispersion or bulge mass (Di Matteo et al. 2005). It is generally believed that the correlations indicate a joint evolution of galaxies and BHs, with BH growth happening at the same time as the bulge growth, and providing a self-regulation via feedback (Silk & Rees 1998; but see Peng 2007 and Jahnke & Macciò 2011 for a non-causal origin of the correlations). We demonstrate that indeed the σ variation directly traces the bulge growth (Kormendy & Gebhardt 2001). In fact σ traces the central galaxy concentration and the bulge size as estimated on optical morphology, while the outer galaxy disks remain flat. This implies that, if the BH indeed accretes from the same gas that grows the bulge, BH mass should correlate better with σ than with total mass as observed (Gebhardt et al. 2000; Ferrarese & Merritt 2000).

However, when ETGs experience dry mergers, their BH grows in proportion to the mass, but galaxies move along lines of nearly constant σ. For this reason, an expectation from this picture is that BHs at the high mass end should start to appear too massive with respect to the predictions of the $M_{\rm BH} - \sigma$ relation (see also Nipoti et al. 2003; Boylan-Kolchin et al. 2006). The high-mass BH end is still not sufficiently populated to reliably test this prediction, but indirect evidence seems to support this possibility (Lauer et al. 2007), as well as the recent detection of two giant black holes at the centre of two bright cluster galaxies, which are clearly more massive than the $M_{\rm BH} - \sigma$ prediction (McConnell et al. 2011).

In summary we propose that the distribution of galaxy properties on the VP, where M/L and age follows lines of constant σ on the VP, could be explained by the combination of two processes, which can happen multiple times during the evolution of a single galaxy: (i) They accrete gas, which grows the bulge and BH, shrinks their $R_{\rm e}$, and increases σ_e and concentration, while some process which seems associated with the bulge growth (e.g. AGN

feedback), quenches star formation; (ii) They experience mostly minor dry mergers that move them along lines of roughly constant σ (or steeper).

An open question in the scenario in which ETGs evolve relatively quietly from spirals comes from the comparison of our findings with the empirical scaling relations one observes at larger redshift. In fact at $z \gtrsim 1.5$ galaxies are found to be smaller than local ones with the same mass (Daddi et al. 2005; Trujillo et al. 2006, 2007; van Dokkum et al. 2008; Cimatti et al. 2008). They populate the region below the ZOE of local galaxies. This may indicate that the compact high-redshift ETGs follow a different and more violent evolutionary path than the more quiet majority of local ETGs (Barro et al. 2012). We show in the top panel of Fig. 2 that the 12 available determinations of σ (Cenarro & Trujillo 2009; Cappellari et al. 2009; van Dokkum et al. 2009; Onodera et al. 2010; van de Sande et al. 2011) are all consistent within the errors with the ATLAS^{3D} VP, with the only exception being the object presented in van Dokkum et al. (2009). A way to reconcile this very mild (or lack of) σ evolution is by assuming that the compact primordial ETGs grow mostly by accretion of small satellites in their outer halos, while preserving the central structure (Naab et al. 2009; Hopkins et al. 2010; Oser et al. 2010, 2012). This seems consistent with the shape of the photometric profiles of the early ETGs (Hopkins et al. 2009a; Bezanson et al. 2009; van Dokkum et al. 2010; Hilz et al. 2012a). A caveat is that significant biases may still exist in the high-redshift photometry (Mancini et al. 2010), considering that systematic differences of up to a factor of two exists even on well observed ETGs in the nearby Universe (Kormendy et al. 2009, Chen et al. 2010, Paper I). Moreover comparisons of photometric profiles tend to be made against bona fide ellipticals, while the remnant of the high-redshift ETGs are likely disk-like fast rotators ETG, which have systematically different profiles. Finally the comparisons should ideally be done in mass density, instead of surface density, but kinematic information is available for only a handful of galaxies. This implies that there is perhaps still some room for the compact high-z ETGs to become more consistent with local ones, than currently assumed.

6 SUMMARY

In the companion Paper XIX we describe in detail the dynamical models for all the ATLAS^{3D} ETGs that were introduced in Cappellari et al. (2012). We found that galaxies lie on a thin Virial Plane (VP) in the three-dimensional parameter space defined by $(M_{\rm JAM}, \sigma_e, R_e^{\rm max})$.

Here we studied the inclined projection of the VP and find that: (i) the location galaxies define a clear boundary, well described by two power-laws, joined by a break at a characteristic mass $M_{\rm JAM} \equiv L \times (M/L)_e \approx 3 \times 10^{10} M_\odot$, which corresponds to the regime where a number of global galaxy properties were reported to change; (ii) The distribution of $(M/L)_e$, as well as population indicators of $(M/L)_{\rm pop}$ like $H\beta$ and colour, together with galaxy concentration that we show here is measuring bulge size, all tend to be constant along lines of constant σ_e.

These findings explains why σ_e (not L, M, $R_{\rm e}$or Σ_e) has often been the most successful single descriptor of galaxy properties. We discuss a number of previously found galaxy correlation and we find that they are all consistent with what we find. In fact most observed relations turn out to be just special projections of the cleaner and more general view provided by the VP.

The stellar initial mass function was previously shown (e.g. Cappellari et al. 2012) to vary systematically with $(M/L)_{\rm stars}$ and as expected it also follows the other population indicators and also tend to vary along lines of nearly constant σ_e on the VP. This is a necessary expectation if one wants to preserve the tightness of the Fundamental Plane or the $(M/L) - \sigma_e$ relation. The trend of IMF with σ appears to account for about half of the total trend in the $(M/L) - \sigma_e$ relation (see Paper XIX), the remaining one being due to stellar population variations.

The distribution of galaxy properties on the VP can be qualitatively interpreted as due to a combination of two main processes: (i) bulge growth, changing the galaxy population and decreasing $R_{\rm e}$, while increasing σ_e, and (ii) dry merging, increasing $R_{\rm e}$ by moving galaxies along lines of approximately constant σ_e, while leaving the population unchanged. It is unclear where the reported dense ETGs fit in this picture. They may simply follow a different route, which forms the most massive galaxies and is not affecting the fast rotator population, which dominates ETGs in the nearby Universe. Or there may be some remaining biases in the photometric observations, producing an underestimation of the radius. The few available high-redshift σ determinations are in fact all with one exception consistent with what we observed on the VP. Stellar kinematics of high-redshift ETGs is critically needed to address this question.

ACKNOWLEDGEMENTS

MC acknowledges support from a Royal Society University Research Fellowship. This work was supported by the rolling grants 'Astrophysics at Oxford' PP/E001114/1 and ST/H002456/1 and visitors grants PPA/V/S/2002/00553, PP/E001564/1 and ST/H504862/1 from the UK Research Councils. RLD acknowledges travel and computer grants from Christ Church, Oxford and support from the Royal Society in the form of a Wolfson Merit Award 502011.K502/jd. RLD also acknowledges the support of the ESO Visitor Programme which funded a 3 month stay in 2010. SK acknowledges support from the Royal Society Joint Projects Grant JP0869822. RMcD is supported by the Gemini Observatory, which is operated by the Association of Universities for Research in Astronomy, Inc., on behalf of the international Gemini partnership of Argentina, Australia, Brazil, Canada, Chile, the United Kingdom, and the United States of America. TN and MBois acknowledge support from the DFG Cluster of Excellence 'Origin and Structure of the Universe'. MS acknowledges support from a STFC Advanced Fellowship ST/F009186/1. PS is a NWO/Veni fellow. (TAD) The research leading to these results has received funding from the European Community's Seventh Framework Programme (/FP7/2007-2013/) under grant agreement No 229517. MBois has received, during this research, funding from the European Research Council under the Advanced Grant Program Num 267399-Momentum. The authors acknowledge financial support from ESO.

REFERENCES

Abadi M. G., Moore B., Bower R. G., 1999, MNRAS, 308, 947
Aihara H., Allende Prieto C., An D., et al., 2011, ApJS, 193, 29
Auger M. W., Treu T., Bolton A. S., Gavazzi R., Koopmans L. V. E., Marshall P. J., Bundy K., Moustakas L. A., 2009, ApJ, 705, 1099
Auger M. W., Treu T., Bolton A. S., Gavazzi R., Koopmans L. V. E., Marshall P. J., Moustakas L. A., Burles S., 2010a, ApJ, 724, 511

Auger M. W., Treu T., Gavazzi R., Bolton A. S., Koopmans L. V. E., Marshall P. J., 2010b, ApJ, 721, L163
Bacon R. et al., 2001, MNRAS, 326, 23
Barnabè M., Czoske O., Koopmans L. V. E., Treu T., Bolton A. S., 2011, MNRAS, 415, 2215
Barnabè M. et al., 2012, MNRAS, 423, 1073
Barro G. et al., 2012, arXiv:1206.5000
Bastian N., R. C. K., Meyer M. R., 2010, ARA&A, 48, 339
Bell E. F., de Jong R. S., 2001, ApJ, 550, 212
Bell E. F. et al., 2012, ApJ, 753, 167
Bender R., Burstein D., Faber S. M., 1992, ApJ, 399, 462
Bender R., Burstein D., Faber S. M., 1993, ApJ, 411, 153
Bernardi M., Roche N., Shankar F., Sheth R. K., 2011, MNRAS, 412, L6
Bernardi M. et al., 2003, AJ, 125, 1866
Bershady M. A., Martinsson T. P. K., Verheijen M. A. W., Westfall K. B., Andersen D. R., Swaters R. A., 2011, ApJ, 739, L47
Bershady M. A., Verheijen M. A. W., Swaters R. A., Andersen D. R., Westfall K. B., Martinsson T., 2010, ApJ, 716, 198
Bezanson R., van Dokkum P. G., Tal T., Marchesini D., Kriek M., Franx M., Coppi P., 2009, ApJ, 697, 1290
Binggeli B., Sandage A., Tarenghi M., 1984, AJ, 89, 64
Binney J., Tremaine S., 2008, Galactic Dynamics: Second Edition. Princeton University Press
Bois M. et al., 2011, MNRAS, 416, 1654 (Paper VI)
Bolton A. S., Burles S., Koopmans L. V. E., Treu T., Gavazzi R., Moustakas L. A., Wayth R., Schlegel D. J., 2008a, ApJ, 682, 964
Bolton A. S., Burles S., Koopmans L. V. E., Treu T., Moustakas L. A., 2006, ApJ, 638, 703
Bolton A. S., Treu T., Koopmans L. V. E., Gavazzi R., Moustakas L. A., Burles S., Schlegel D. J., Wayth R., 2008b, ApJ, 684, 248
Bournaud F., Elmegreen B. G., Elmegreen D. M., 2007, ApJ, 670, 237
Boylan-Kolchin M., Ma C.-P., Quataert E., 2006, MNRAS, 369, 1081
Brewer B. J. et al., 2012, MNRAS, 422, 3574
Burstein D., Bender R., Faber S., Nolthenius R., 1997, AJ, 114, 1365
Burstein D., Davies R. L., Dressler A., Faber S. M., Lynden-Bell D., 1988, in Astrophysics and Space Science Library, Vol. 141, Towards Understanding Galaxies at Large Redshift, Renzini R. G. K. . A., ed., pp. 17–21
Caon N., Capaccioli M., D'Onofrio M., 1993, MNRAS, 265, 1013
Cappellari M., 2002, MNRAS, 333, 400
Cappellari M., 2008, MNRAS, 390, 71
Cappellari M., 2011a, in Paper presented at the conference on Galaxy Formation held 18–22 July, 2011 at Durham University, Durham, UK. Online at http://astro.dur.ac.uk/Gal2011/talks.php
Cappellari M., 2011b, Nature, 480, 187
Cappellari M. et al., 2006, MNRAS, 366, 1126
Cappellari M. et al., 2009, ApJ, 704, L34
Cappellari M., Emsellem E., 2004, PASP, 116, 138
Cappellari M. et al., 2007, MNRAS, 379, 418
Cappellari M. et al., 2011a, MNRAS, 413, 813 (Paper I)
Cappellari M. et al., 2011b, MNRAS, 416, 1680 (Paper VII)
Cappellari M. et al., 2012, Nature, 484, 485
Carlberg R. G., 1986, ApJ, 310, 593
Cenarro A. J., Gorgas J., Vazdekis A., Cardiel N., Peletier R. F., 2003, MNRAS, 339, L12
Cenarro A. J., Trujillo I., 2009, ApJ, 696, L43
Chabrier G., 2003, PASP, 115, 763
Chen C., Côté P., West A. A., Peng E. W., Ferrarese L., 2010, ApJS, 191, 1
Cimatti A. et al., 2008, A&A, 482, 21
Ciotti L., 1991, A&A, 249, 99
Ciotti L., Lanzoni B., Volonteri M., 2007, ApJ, 658, 65
Cleveland W., 1979, Journal of the American statistical association, 829
Cleveland W., Devlin S., 1988, Journal of the American Statistical Association, 596
Cody A. M., Carter D., Bridges T. J., Mobasher B., Poggianti B. M., 2009, MNRAS, 396, 1647
Cole S., Lacey C. G., Baugh C. M., Frenk C. S., 2000, MNRAS, 319, 168
Conroy C., Gunn J. E., White M., 2009, ApJ, 699, 486
Conroy C., van Dokkum P., 2012a, ApJ, 747, 69
Conroy C., van Dokkum P., 2012b, arXiv:1205.6473
Daddi E. et al., 2010, ApJ, 713, 686
Daddi E. et al., 2005, ApJ, 626, 680
Davé R., 2008, MNRAS, 385, 147
Davies R. L., Efstathiou G., Fall S. M., Illingworth G., Schechter P. L., 1983, ApJ, 266, 41
Davies R. L., Sadler E. M., Peletier R. F., 1993, MNRAS, 262, 650
de Rijcke S., Michielsen D., Dejonghe H., Zeilinger W. W., Hau G. K. T., 2005, A&A, 438, 491
de Vaucouleurs G., 1959, Handbuch der Physik, 53, 311
de Zeeuw P. T. et al., 2002, MNRAS, 329, 513
Deason A. J., Belokurov V., Evans N. W., McCarthy I. G., 2012, ApJ, 748, 2
Dekel A. et al., 2009, Nature, 457, 451
Dekel A., Silk J., 1986, ApJ, 303, 39
Di Matteo T., Springel V., Hernquist L., 2005, Nature, 433, 604
Djorgovski S., Davis M., 1987, ApJ, 313, 59
D'Onofrio M. et al., 2008, ApJ, 685, 875
D'Onofrio M. et al., 2011, ApJ, 727, L6+
Dressler A., 1980, ApJ, 236, 351
Dressler A., Lynden-Bell D., Burstein D., Davies R. L., Faber S. M., Terlevich R., Wegner G., 1987, ApJ, 313, 42
Driver S. P. et al., 2011, MNRAS, 413, 971
Dutton A. A. et al., 2011a, MNRAS, 417, 1621
Dutton A. A. et al., 2011b, MNRAS, 416, 322
Dutton A. A., Maccio' A. V., Mendel J. T., Simard L., 2012a, arXiv:1204.2825
Dutton A. A., Mendel J. T., Simard L., 2012b, MNRAS, 422, L33
Dutton A. A. et al., 2012c, arXiv:1206.4310
Elmegreen D. M., Elmegreen B. G., Ravindranath S., Coe D. A., 2007, ApJ, 658, 763
Emsellem E. et al., 2007, MNRAS, 379, 401
Emsellem E. et al., 2004, MNRAS, 352, 721
Emsellem E., Monnet G., Bacon R., 1994, A&A, 285, 723
Faber S. M. et al., 1997, AJ, 114, 1771
Faber S. M., Dressler A., Davies R. L., Burstein D., Lynden-Bell D., 1987, in Nearly Normal Galaxies. From the Planck Time to the Present, Faber S. M., ed., pp. 175–183
Faber S. M., Jackson R. E., 1976, ApJ, 204, 668
Falcón-Barroso J., Sánchez-Blázquez P., Vazdekis A., Ricciardelli E., Cardiel N., Cenarro A. J., Gorgas J., Peletier R. F., 2011, A&A, 532, A95
Ferrarese L. et al., 2006, ApJ, 644, L21
Ferrarese L., Merritt D., 2000, ApJ, 539, L9
Ferreras I., La Barbera F., de Carvalho R. R., de la Rosa

I. G., Vazdekis A., Falcon-Barroso J., Ricciardelli E., 2012, arXiv:1206.1594
Ferreras I., Saha P., Burles S., 2008, MNRAS, 383, 857
Ferreras I., Saha P., Leier D., Courbin F., Falco E. E., 2010, MNRAS, 409, L30
Forbes D. A., Lasky P., Graham A. W., Spitler L., 2008, MNRAS, 389, 1924
Forbes D. A., Spitler L. R., Graham A. W., Foster C., Hau G. K. T., Benson A., 2011, MNRAS, 413, 2665
Förster Schreiber N. M. et al., 2009, ApJ, 706, 1364
Förster Schreiber N. M. et al., 2006, ApJ, 645, 1062
Franx M., van Dokkum P. G., Schreiber N. M. F., Wuyts S., Labbé I., Toft S., 2008, ApJ, 688, 770
Gallazzi A., Bell E. F., 2009, ApJS, 185, 253
Gallazzi A., Charlot S., Brinchmann J., White S. D. M., 2006, MNRAS, 370, 1106
Gargiulo A. et al., 2009, MNRAS, 397, 75
Gavazzi G., Donati A., Cucciati O., Sabatini S., Boselli A., Davies J., Zibetti S., 2005, A&A, 430, 411
Gavazzi R., Treu T., Rhodes J. D., Koopmans L. V. E., Bolton A. S., Burles S., Massey R. J., Moustakas L. A., 2007, ApJ, 667, 176
Gebhardt K. et al., 2000, ApJ, 539, L13
Geha M., Blanton M., Yan R., Tinker J., 2012, arXiv:1206.3573
Gelman A., Carlin J., Stern H., Rubin D., 2004, Bayesian data analysis. CRC press
Genel S. et al., 2012, ApJ, 745, 11
Genzel R. et al., 2011, ApJ, 733, 101
Gerhard O., Kronawitter A., Saglia R. P., Bender R., 2001, AJ, 121, 1936
Gnedin O. Y., Ceverino D., Gnedin N. Y., Klypin A. A., Kravtsov A. V., Levine R., Nagai D., Yepes G., 2011, arXiv:1108.5736
Gnedin O. Y., Kravtsov A. V., Klypin A. A., Nagai D., 2004, ApJ, 616, 16
Governato F. et al., 2010, Nature, 463, 203
Graham A. W., 2004, ApJ, 613, L33
Graham A. W., 2011, in Planets, stars and stellar systems, Springer in press
Graham A. W., Erwin P., Caon N., Trujillo I., 2001a, ApJ, 563, L11
Graham A. W., Guzmán R., 2003, AJ, 125, 2936
Graham A. W., Trujillo I., Caon N., 2001b, AJ, 122, 1707
Graham A. W., Worley C. C., 2008, MNRAS, 388, 1708
Graves G. J., Faber S. M., 2010, ApJ, 717, 803
Graves G. J., Faber S. M., Schiavon R. P., 2009, ApJ, 698, 1590
Grillo C., Gobat R., 2010, MNRAS, 402, L67
Grillo C., Gobat R., Lombardi M., Rosati P., 2009, A&A, 501, 461
Gunawardhana M. L. P. et al., 2011, MNRAS, 415, 1647
Heavens A., Panter B., Jimenez R., Dunlop J., 2004, Nature, 428, 625
Hernquist L., 1990, ApJ, 356, 359
Hernquist L., Spergel D. N., Heyl J. S., 1993, ApJ, 416, 415
Hilz M., Naab T., Ostriker J. P., 2012a, arXiv:1206.5004
Hilz M., Naab T., Ostriker J. P., Thomas J., Burkert A., Jesseit R., 2012b, arXiv:1206.1597
Hopkins P. F., Bundy K., Hernquist L., Wuyts S., Cox T. J., 2010, MNRAS, 401, 1099
Hopkins P. F., Bundy K., Murray N., Quataert E., Lauer T. R., Ma C.-P., 2009a, MNRAS, 398, 898
Hopkins P. F., Hernquist L., Cox T. J., Keres D., Wuyts S., 2009b, ApJ, 691, 1424
Hopkins P. F., Keres D., Murray N., Quataert E., Hernquist L., 2011, ArXiv e-prints
Hoversten E. A., Glazebrook K., 2008, ApJ, 675, 163
Hubble E. P., 1936, Realm of the Nebulae. Yale Univ. Press, New Haven
Huchra J., Gorenstein M., Kent S., Shapiro I., Smith G., Horine E., Perley R., 1985, AJ, 90, 691
Hyde J. B., Bernardi M., 2009a, MNRAS, 394, 1978
Hyde J. B., Bernardi M., 2009b, MNRAS, 396, 1171
Jaffe W., 1983, MNRAS, 202, 995
Jahnke K., Macciò A. V., 2011, ApJ, 734, 92
Janz J., Lisker T., 2008, ApJ, 689, L25
Jiang F., van Dokkum P., Bezanson R., Franx M., 2012, ApJ, 749, L10
Kassin S. A., de Jong R. S., Weiner B. J., 2006, ApJ, 643, 804
Kauffmann G. et al., 2003a, MNRAS, 341, 33
Kauffmann G. et al., 2003b, MNRAS, 341, 54
Kelly B. C., 2007, ApJ, 665, 1489
Kelson D. D., van Dokkum P. G., Franx M., Illingworth G. D., Fabricant D., 1997, ApJ, 478, L13
Kennicutt, Jr. R. C., 1998, in Astronomical Society of the Pacific Conference Series, Vol. 142, The Stellar Initial Mass Function (38th Herstmonceux Conference), Howell G. G. . D., ed., p. 1
Khochfar S. et al., 2011, MNRAS, 417, 845 (Paper VIII)
Khochfar S., Ostriker J. P., 2008, ApJ, 680, 54
Khochfar S., Silk J., 2006, MNRAS, 370, 902
Koopmans L. V. E., Treu T., Bolton A. S., Burles S., Moustakas L. A., 2006, ApJ, 649, 599
Kormendy J., 1977, ApJ, 218, 333
Kormendy J., 1985, ApJ, 295, 73
Kormendy J., Bender R., 2012, ApJS, 198, 2
Kormendy J., Fisher D. B., Cornell M. E., Bender R., 2009, ApJS, 182, 216
Kormendy J., Gebhardt K., 2001, in American Institute of Physics Conference Series, Vol. 586, 20th Texas Symposium on relativistic astrophysics, Wheeler J. C., Martel H., eds., pp. 363–+
Kormendy J., Kennicutt, Jr. R. C., 2004, ARA&A, 42, 603
Krajnović D. et al., 2012, MNRAS, submitted (Paper XVII)
Kroupa P., 2001, MNRAS, 322, 231
Kroupa P., 2002, Science, 295, 82
Kroupa P., Weidner C., 2003, ApJ, 598, 1076
Kroupa P., Weidner C., Pflamm-Altenburg J., Thies I., Dabringhausen J., Marks M., Maschberger T., 2012, arXiv:1112.3340
Kuntschner H. et al., 2006, MNRAS, 369, 497
Kuntschner H., Emsellem E., et al., 2010, MNRAS, 408, 97
Lablanche P.-Y. et al., 2012, MNRAS, 424, 1495 (Paper XII)
Lauer T. R. et al., 2007, ApJ, 662, 808
Law D. R., Shapley A. E., Steidel C. C., Reddy N. A., Christensen C. R., Erb D. K., 2012, Nature, 487, 338
Longhetti M., Saracco P., 2009, MNRAS, 394, 774
Magorrian J. et al., 1998, AJ, 115, 2285
Mancini C. et al., 2010, MNRAS, 401, 933
Maraston C., 2005, MNRAS, 362, 799
Maraston C., Daddi E., Renzini A., Cimatti A., Dickinson M., Papovich C., Pasquali A., Pirzkal N., 2006, ApJ, 652, 85
Martig M., Bournaud F., Teyssier R., Dekel A., 2009, ApJ, 707, 250
Matković A., Guzmán R., 2005, MNRAS, 362, 289
McConnell N. J., Ma C.-P., Gebhardt K., Wright S. A., Murphy J. D., Lauer T. R., Graham J. R., Richstone D. O., 2011, Nature, 480, 215
Mei S. et al., 2007, ApJ, 655, 144
Mihos J. C., Hernquist L., 1994, ApJ, 431, L9

Misgeld I., Hilker M., 2011, MNRAS, 414, 3699
Moster B. P., Somerville R. S., Maulbetsch C., van den Bosch F. C., Macciò A. V., Naab T., Oser L., 2010, ApJ, 710, 903
Naab T., Johansson P. H., Ostriker J. P., 2009, ApJ, 699, L178
Napolitano N. R., Romanowsky A. J., Tortora C., 2010, MNRAS, 405, 2351
Navarro J. F., Frenk C. S., White S. D. M., 1996, ApJ, 462, 563
Nipoti C., Londrillo P., Ciotti L., 2003, MNRAS, 342, 501
Nipoti C., Treu T., Auger M. W., Bolton A. S., 2009, ApJ, 706, L86
Onodera M. et al., 2010, ApJ, 715, L6
Onodera M. et al., 2012, ApJ, 755, 26
Oser L., Naab T., Ostriker J. P., Johansson P. H., 2012, ApJ, 744, 63
Oser L., Ostriker J. P., Naab T., Johansson P. H., Burkert A., 2010, ApJ, 725, 2312
Padmanabhan N. et al., 2004, New Astr., 9, 329
Peng C. Y., 2007, ApJ, 671, 1098
Press W. H., Teukolsky S. A., Vetterling W. T., Flannery B. P., 1992, Numerical recipes in FORTRAN. The art of scientific computing. Cambridge: University Press, —c1992, 2nd ed.
Prugniel P., Simien F., 1996, A&A, 309, 749
Renzini A., 2005, in Astrophysics and Space Science Library, Vol. 327, The Initial Mass Function 50 Years Later, Corbelli E., Palla F., Zinnecker H., eds., p. 221
Renzini A., Ciotti L., 1993, ApJ, 416, L49+
Robertson B., Cox T. J., Hernquist L., Franx M., Hopkins P. F., Martini P., Springel V., 2006, ApJ, 641, 21
Salpeter E. E., 1955, ApJ, 121, 161
Sánchez-Blázquez P. et al., 2006, MNRAS, 371, 703
Sandage A., 1961, The Hubble Atlas. Carnegie Institution, Washington
Sarzi M., Shields J. C., et al., 2010, MNRAS, 402, 2187
Schechter P., 1976, ApJ, 203, 297
Schiavon R. P., Barbuy B., Bruzual A. G., 2000, ApJ, 532, 453
Schulz A. E., Mandelbaum R., Padmanabhan N., 2010, MNRAS, 408, 1463
Scott N. et al., 2009, MNRAS, 398, 1835
Scott N. et al., 2012, MNRAS, submitted (Paper XXI)
Sersic J. L., 1968, Atlas de galaxias australes. Cordoba, Argentina: Observatorio Astronomico, 1968
Shankar F., Bernardi M., 2009, MNRAS, 396, L76
Silk J., Rees M. J., 1998, A&A, 331, L1
Skrutskie M. F. et al., 2006, AJ, 131, 1163
Smith R. J., Lucey J. R., Carter D., 2012, arXiv:1206.4311
Sonnenfeld A., Treu T., Gavazzi R., Marshall P. J., Auger M. W., Suyu S. H., Koopmans L. V. E., Bolton A. S., 2012, ApJ, 752, 163
Spiniello C., Trager S. C., Koopmans L. V. E., Chen Y. P., 2012, ApJ, 753, L32
Spinrad H., Taylor B. J., 1971, ApJS, 22, 445
Spitzer, Jr. L., Baade W., 1951, ApJ, 113, 413
Suyu S. H. et al., 2012, ApJ, 750, 10
Tacconi L. J. et al., 2010, Nature, 463, 781
Thomas D., Maraston C., Bender R., Mendes de Oliveira C., 2005, ApJ, 621, 673
Thomas J., Saglia R. P., Bender R., Thomas D., Gebhardt K., Magorrian J., Corsini E. M., Wegner G., 2009, ApJ, 691, 770
Thomas J. et al., 2011, MNRAS, 415, 545
Tonry J. L., 1981, ApJ, 251, L1
Tonry J. L., Dressler A., Blakeslee J. P., Ajhar E. A., Fletcher A. B., Luppino G. A., Metzger M. R., Moore C. B., 2001, ApJ, 546, 681
Tortora C., Napolitano N. R., Romanowsky A. J., Capaccioli M., Covone G., 2009, MNRAS, 396, 1132
Tortora C., Napolitano N. R., Romanowsky A. J., Jetzer P., 2010, ApJ, 721, L1
Tortora C., Romanowsky A. J., Napolitano N. R., 2012, arXiv:1207.4475
Tremblay B., Merritt D., 1996, AJ, 111, 2243
Treu T., Auger M. W., Koopmans L. V. E., Gavazzi R., Marshall P. J., Bolton A. S., 2010, ApJ, 709, 1195
Treu T., Dutton A. A., Auger M. W., Marshall P. J., Bolton A. S., Brewer B. J., Koo D. C., Koopmans L. V. E., 2011, MNRAS, 417, 1601
Treu T. et al., 2005, ApJ, 633, 174
Trujillo I., Conselice C. J., Bundy K., Cooper M. C., Eisenhardt P., Ellis R. S., 2007, MNRAS, 382, 109
Trujillo I., Ferreras I., de La Rosa I. G., 2011, MNRAS, 938
Trujillo I. et al., 2006, MNRAS, 373, L36
Trujillo I., Graham A. W., Caon N., 2001, MNRAS, 326, 869
Valentinuzzi T. et al., 2010, ApJ, 712, 226
van de Sande J. et al., 2011, ApJ, 736, L9+
van de Ven G., Falcón-Barroso J., McDermid R. M., Cappellari M., Miller B. W., de Zeeuw P. T., 2010, ApJ, 719, 1481
van den Bergh S., 1976, ApJ, 206, 883
van der Marel R. P., van Dokkum P. G., 2007, ApJ, 668, 756
van der Wel A., Bell E. F., van den Bosch F. C., Gallazzi A., Rix H.-W., 2009a, ApJ, 698, 1232
van der Wel A., Rix H.-W., Holden B. P., Bell E. F., Robaina A. R., 2009b, ApJ, 706, L120
van der Wel A. et al., 2011, ApJ, 730, 38
van Dokkum P., 2011, Nature, 473, 160
van Dokkum P., Conroy C., 2012, arXiv:1205.6471
van Dokkum P. G., 2008, ApJ, 674, 29
van Dokkum P. G., Conroy C., 2010, Nature, 468, 940
van Dokkum P. G., Conroy C., 2011, ApJ, 735, L13
van Dokkum P. G., Franx M., 1996, MNRAS, 281, 985
van Dokkum P. G., Franx M., Kelson D. D., Illingworth G. D., 1998, ApJ, 504, L17
van Dokkum P. G. et al., 2008, ApJ, 677, L5
van Dokkum P. G., Kriek M., Franx M., 2009, Nature, 460, 717
van Dokkum P. G. et al., 2010, ApJ, 709, 1018
Vazdekis A., Ricciardelli E., Cenarro A. J., Rivero-González J. G., Díaz-García L. A., Falcón-Barroso J., 2012, MNRAS, 424, 157
Vazdekis A., Sánchez-Blázquez P., Falcón-Barroso J., Cenarro A. J., Beasley M. A., Cardiel N., Gorgas J., Peletier R. F., 2010, MNRAS, 404, 1639
Wake D. A., van Dokkum P. G., Franx M., 2012, ApJ, 751, L44
Wegner G. A., Corsini E. M., Thomas J., Saglia R. P., Bender R., Pu S. B., 2012, AJ, 144, 78
Wilkins S. M., Hopkins A. M., Trentham N., Tojeiro R., 2008, MNRAS, 391, 363
Williams M. J., Bureau M., Cappellari M., 2009, MNRAS, 400, 1665
Williams M. J., Bureau M., Cappellari M., 2010, MNRAS, 409, 1330
Wolf J., Martinez G. D., Bullock J. S., Kaplinghat M., Geha M., Muñoz R. R., Simon J. D., Avedo F. F., 2010, MNRAS, 406, 1220
Worthey G., 1994, ApJS, 95, 107
Wuyts S., Franx M., Cox T. J., Hernquist L., Hopkins P. F., Robertson B. E., van Dokkum P. G., 2009, ApJ, 696, 348

York D. G., Adelman J., Anderson, Jr. J. E., et al., 2000, AJ, 120, 1579
Young L. M. et al., 2011, MNRAS, 414, 940 (Paper IV)
Zaritsky D., Gonzalez A. H., Zabludoff A. I., 2006, ApJ, 638, 725
Zhu G., Blanton M. R., Moustakas J., 2010, ApJ, 722, 491